TNO Physics and Electronics Labor

Oude W
2597 A
P.O. Box 96864
2509 JG The Hague
The Netherlands

Fax +31 70 328 09 61
Phone +31 70 326 42 21

(1)

TNO-report copy no.

FEL-93-A035 1

title

Conversion of the CLUSE model for applications over open ocean; progress report

author(s):
Dr. A.M.J. van Eijk
Dr. P.G. Mestayer*
Dr. G. de Leeuw

* Equipe Dynamique de l'Atmosphère Habitée
Laboratoire de Mécanique des Fluides
Ecole Centrale de Nantes, France

date:
August 1993

classification

classified by	: W. Pelt
classification date	: August 6, 1993
title	: ongerubriceerd
abstract	: ongerubriceerd
report text	: ongerubriceerd
appendices A - E	: ongerubriceerd

no. of copies	: 37
no. of pages	: 79 (including appendices, excluding RDP and distribution list)
no. of appendices	: 5

All information which is classified according to Dutch regulations shall be treated by the recipient in the same way as classified information of corresponding value in his own country. No part of this information will be disclosed to any party.

The classification designation ONGERUBRICEERD is equivalent to UNCLASSIFIED.

Netherlands organization for applied scientific research

TNO Defence Research consists of:
the TNO Physics and Electronics Laboratory,
the TNO Prins Maurits Laboratory and the

The Standard Conditions for Research Instructions given to TNO, as filed at the Registry of the District Court and the Chamber of Commerce in The Hague

report no. : FEL-93-A035

title : Conversion of the CLUSE model for applications over open ocean; progress report

author(s) : Dr. A.M.J. van Eijk, Dr. P.G. Mestayer, Dr. G. de Leeuw

institute : TNO Physics and Electronics Laboratory

date : August 1993

NDRO no. : A90KM638

no. in pow '93 : 766.1

Research supervised by : Dr. P.G. Mestayer, Dr. G. de Leeuw

Research carried out by : Dr. A.M.J. van Eijk

ABSTRACT (ONGERUBRICEERD)

The CLUSE model has been developed to describe the dynamics of (fresh water) spray droplets in the homogeneous boundary layer of an air-sea interaction simulation tunnel, and their influence on humidity and temperature profiles [Rouault et al., 1991]. Extension to open ocean conditions requires that the fresh water droplets are replaced by sea-salt aerosol, and that the influence of waves is taken into account. In this report we describe the progress on the development of the SeaCluse model that applies to open ocean conditions. The calculation of the profiles of the mean wind velocity and turbulent diffusivity has been changed to take into account the characteristics of the marine atmosphere and of the wave field. A module was added to the initialization routines that models the air flow over the waves in a non-turbulent and non-evaporative atmosphere. This module yields vertical profiles of droplet concentrations that enter in the relaxation term that models the mean movement of the particles. These profiles are then modified in the iterative budget calculation that accounts for droplet transport by atmospheric turbulence and their interaction with the humidity field by evaporation. In this part of the code, the evaporation module was changed to describe the evaporation of sea salt aerosols in the marine atmosphere. The output of the new SeaCluse model consists of vertical profiles of temperature, humidity and aerosol concentration from the sea surface up to the top of the marine atmospheric boundary layer.

rapport no.	:	FEL-93-A035
titel	:	Conversie van het CLUSE model voor toepassing in 'open ocean' condities; voortgangsrapport
auteur(s)	:	Dr. A.M.J. van Eijk, Dr. P.G. Mestayer, Dr. G. de Leeuw
instituut	:	Fysisch en Elektronisch Laboratorium TNO
datum	:	augustus 1993
hdo-opdr.no.	:	A90KM638
no. in iwp '93	:	766.1
Onderzoek uitgevoerd o.l.v.	:	Dr. P.G. Mestayer, Dr. G. de Leeuw
Onderzoek uitgevoerd door	:	Dr. A.M.J. van Eijk

SAMENVATTING (ONGERUBRICEERD)

Het CLUSE model werd ontwikkeld om de dynamica van (zoet water) spray druppeltjes in de 1-dimensionale homogene grenslaag van een lucht-water interactie tunnel te beschrijven, alsmede de invloed van de waterdruppeltjes op de vochtigheids- en temperatuurprofielen [Rouault et al., 1991]. Voor de uitbreiding van het model naar 'open ocean' condities is vereist dat de zoet water druppels vervangen worden door zeezout aerosolen, en dat de invloed van de golven wordt gemodelleerd. In dit rapport wordt de voortgang beschreven van het geschikt maken van het CLUSE model voor toepassing in 'open ocean' condities. De berekening van de verticale profielen van de gemiddelde windsnelheid en de turbulente diffusie coefficient zijn aangepast aan een maritieme atmosfeer en golven. De initialisatie van het model is uitgebreid met een module waarin de luchtstroming over de golven wordt beschreven in een atmosfeer, waarin geen turbulentie of verdamping voorkomt. Deze module berekent de concentratie profielen van het aerosol die gebruikt worden in de relaxatie term die de gemiddelde beweging van de deeltjes beschrijft. Deze concentratie profielen worden vervolgens gewijzigd in een iteratieve budget berekening, waarbij transport van het aerosol door atmosferische turbulentie en verdamping van het aerosol wordt gemodelleerd. De module die de verdamping van de aerosol deeltjes beschrijft, werd aangepast voor zeezout aerosolen in de mariene atmosfeer. De resultaten van het nieuwe SeaCluse model bestaan uit de verticale profielen van temperatuur, vochtigheid en aerosol concentratie vanaf het zee oppervlak tot aan de top van de mariene grenslaag.

CONTENTS

1 INTRODUCTION

Aerosols play an important role in the marine boundary layer, both in meteorological processes and in the field of propagation of electro-optical radiation. Suspended aerosols, by scattering and absorption of radiation, contribute to the attenuation of radiation in the electromagnetic transmission windows. This reduces the performance of electro-optical systems and limits electro-optical surveillance of the marine boundary layer and the sea surface from aircrafts and satellites. The reduced albedo may also be of importance for climatological studies.

On a micro-meteorological scale, aerosols contribute to the moisture and heat budgets near the sea surface [Wu, 1974; Ling and Kao, 1976; Andreas, 1992]. Since the ocean acts both as a source and a sink for atmospheric aerosols, the aerosol droplets may transfer water vapor, heat, pollutants and bacteria through the air-sea interface. At higher levels, sea-salt particles shrink by evaporation or grow by condensation trough interaction with the humidity field. Hence, they play a role in the transport of matter, heat and water vapor through the marine boundary layer and are important to larger scale meteorological processes and climatology. In addition, small droplets may act as condensation nuclei and are therefore important in the formation of fog and clouds.

In view of the above, adequate descriptions of the particle size distributions for the ambient atmospheric conditions are required to explain a wide range of processes in the marine atmospheric boundary layer. The Navy Aerosol Model (NAM) [Gathman, 1983] is one of the most widely accepted and used models to assess the propagation characteristics of electro-magnetic radiation. It is the maritime version of the LOWTRAN code [Kneizys et.al., 1983]. NAM is an empirical model, based on an extensive data set including a variety of geographical locations. Over the years, NAM has been updated and improved with both experimental [De Leeuw, 1986] and theoretical [Gerber, 1985] evidence [Hughes, 1987; Gathman, 1989].

NAM applies to a single height of 10 m above mean sea level (AMSL). Therefore, additional modeling is required to infer the vertical profiles of aerosol concentration. To this end the Navy Oceanic Vertical Aerosol Model [Gathman, 1989; De Leeuw et.al., 1989a] is being developed. In NOVAM, the concentration of aerosol at deck height is provided by NAM, and the vertical distribution of aerosols is subsequently calculated with physical equations.

Although NAM and NOVAM provide us with valuable information, they cannot be used below 10 m AMSL. Yet, this region is important, because an appreciable part of the propagation path for detection of targets low above the horizon may be below 10 m AMSL. The region is also important for climatological studies, because the coupling terms between atmosphere and ocean in global climate models are not yet ascertained. As described above, an important part of the aerosol dynamics also takes place in the surface layer. Therefore, any model that is developed for the marine atmospheric boundary layer requires a detailed description of the processes near the air-sea interface.

The processes near the air-sea interface are difficult to assess, because they consist of a large number of coupled dynamical and physical processes. When wave breaking occurs, air is entrained into the water. The air breaks up in bubbles, which rise due to their buoyancy. When they reach the surface and burst, sea-spray aerosol is produced (see figure 1.1). Sea spray consists of small film droplets, which result from the breaking of the thin water film covering the bubble when it protrudes the water surface, and jet droplets, which result from the breaking up of the jet that is subsequently formed.

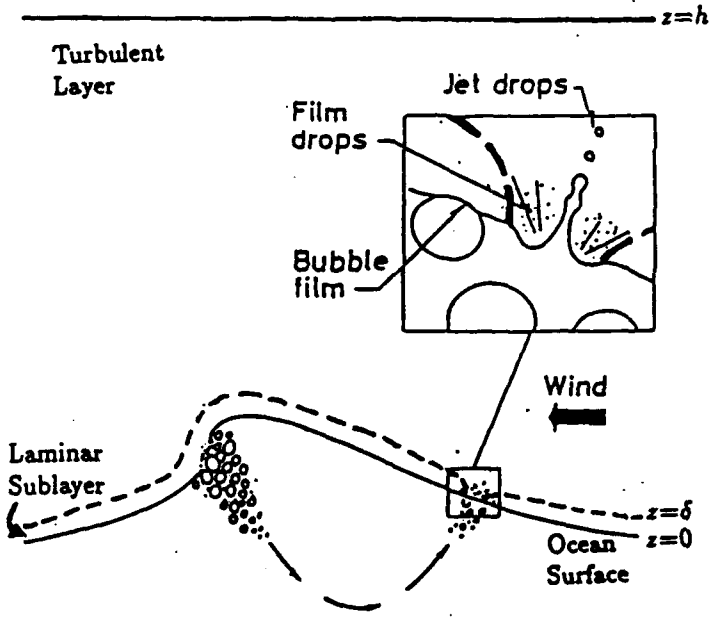

Figure 1.1: Sketch of breaking waves with bubble and spray droplet formation (from [Larsen et al., 1990])

The production of film and jet droplets from both single bubbles and bubble plumes has been the subject of extensive experimental studies (see e.g., Blanchard [1963, 1983], Monahan et.al. [1982], Mestayer and Lefauconnier [1988], Spiel [1992a]). An analytical description of the jet droplet production has recently been provided [Dekker and De Leeuw, 1993], based on analysis by MacIntyre [1968, 1972]. In addition to the film and jet droplets, the so-called spume droplets are produced by wave crest tearing when the wind speed exceeds 9 m/s [Monahan et.al., 1986; Wu, 1990; Andreas, 1992].

The number and size distribution of sea spray aerosols that is produced is given by the droplet source function. Monahan et al. [1982] presented a source function that consists of two modes, that is, a bubble-mediated and a spume droplet source function. Alternative formulations have been given by Fairall et.al. [1983] (see also Miller and Fairall [1988]), De Leeuw [1990a] and Andreas [1992].

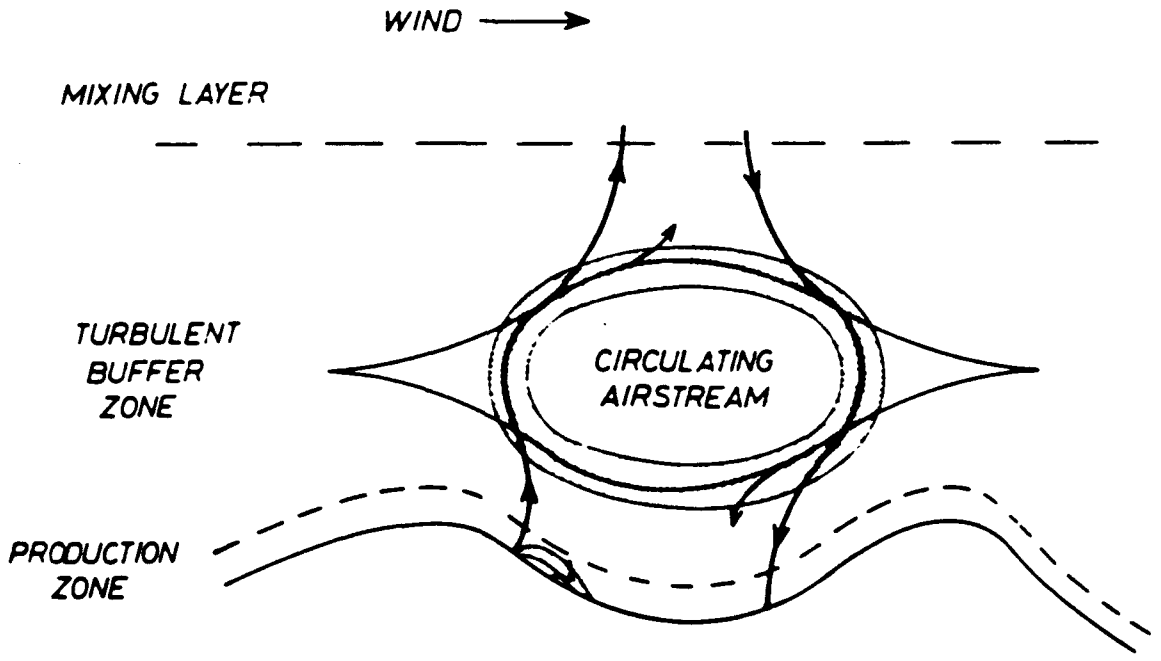

Figure 1.2: Schematic representation of the wave-rotor model

However, it is very difficult to obtain pertinent measurements of the upward surface flux of droplets at sea and the extension of laboratory results to oceanic conditions is not straightforward either. As a result, there is not yet a consensus source function available. In particular, the contribution of spume droplets has by no means been established [Katsaros and De Leeuw, 1993].

The freshly produced droplets are transported upward by turbulent diffusion and convective flow, counterbalanced by gravitational forces. While they are airborne, they interact with the scalar fields of temperature and humidity by heat exchange, evaporation and condensational growth.

Few measurements exist of the concentration of aerosols below ship deck level (see De Leeuw [1989b, 1993] for a review). Until recently the particle concentrations were assumed to increase exponentially toward the sea surface [Blanchard and Woodcock, 1980]. De Leeuw [1986, 1987] provided experimental evidence that the profiles are not always logarithmic and hypothesized a wave-rotor model to explain this behavior (see figure 1.2). According to that model, the aerosols are temporarily trapped in eddies, which results in longer suspension times. Alternatively, Wu [1990] suggested that the spume droplet production by the wave tearing mechanism was to be held responsible for the non-logarithmic profiles.

This discussion shows that there is a requirement for a model that gives a physical description of the behavior of marine spray droplets in the atmospheric surface layer close to the waves, and that provides an adequate explanation for the (sparse) experimental observations. Over the years, various interesting models have been reported (see Rouault et.al. [1991] for an overview), but a detailed description of the behaviour of droplets close to the surface has not yet been given.

In 1981, the Humidity Exchange Over the Sea (HEXOS) program was initiated to study the water vapor and droplet fluxes from sea to air (see Smith et.al. [1990] for a description). The HEXOS studies in a Simulation Tunnel (HEXIST) subprogram was aimed at the development of numerical models to study the turbulent transport of evaporating droplets and their interactions with the scalar fields of temperature and humidity. The measurements which would provide the basis for the model formulations were performed in the period 1985-1990 in the Large Air-Sea Interaction Simulation Tunnel of the Institut de Mécanique Statistique de la Turbulence (IMST) laboratory at Luminy (Marseille, France), and in the whitecap simulation tank at the University of Connecticut (see, e.g., Mestayer et.al. [1988]).

It was recognized that breaking waves in a laboratory tunnel cannot provide a good simulation of the net production of aerosols and water vapor over ocean waves [Mestayer and Lefauconnier, 1988]. Therefore, the tunnel was operated in an artificial configuration, where the surface sources of droplets were provided by bubble plumes generated by immersed aeration devices, where there were no waves and where the air flow was a well-known fully turbulent boundary layer over a flat water surface.

Two different types of models were developed:

(a) A Lagrangian Monte Carlo type simulation of droplet trajectories [Edson, 1989];
(b) An Eulerian K-diffusivity model [Rouault et.al., 1991].

Although fundamentally different, given the same initial conditions, the results from the two models show excellent agreement between each other and with the tunnel measurements. We will not further discuss Edson's model in this report, but restrict ourselves to the Eulerian model (b).

The Couche Limite Unidimensionelle Stationnaire d'Embruns (CLUSE) model by Rouault et al. considers fresh water jet droplets between 5 and 105 μm in radius, ejected from the water surface by bursting bubbles. The model is tuned by an experimental source function. The droplets are then dispersed in a fully developed boundary layer by turbulence over a flat air-water interface. The diffusion by air turbulence is represented by a K-diffusivity term and gravitational and inertial effects are explicitly modeled. The droplet population is split in size bins (categories). Each droplet category is allowed to interact with the ambient humid air. Source-sink functions in the budget equations for the mass concentration of each droplet category, for the water vapor concentration, and for the sensible heat represent the effects of droplet evaporation: transfer between droplet categories due to shrinking, production of water vapor and absorption of sensible heat. A brief summary of the original CLUSE hypotheses and model equations is presented in chapter 2 of this report.

The CLUSE model could successfully demonstrate some of the mechanisms of the non-linear interaction between injection, evaporation, turbulent diffusion and transport of spray droplets [Mestayer, 1990; Rouault et.al., 1991]. However, since it was developed for artificial conditions in a wind-wave interaction tunnel (see above), the CLUSE model must be extended to open ocean conditions before it can describe the behavior of marine spray droplets.

The further development of the CLUSE model for application over sea is a joint effort of the TNO Physics and Electronics Laboratory and the Ecole Centrale de Nantes. Initially, the model code was optimized and made more flexible to allow introduction of open ocean conditions [De Leeuw, et.al., 1991]. The extension of CLUSE to SeaCluse then requires three basic steps. One has to provide:

(a) a model for the air flow over the waves
(b) an evaporation module for sea water droplets
(c) a source function for open ocean conditions

The present efforts are mainly aimed at (a) and (b). We describe the air flow over the waves by a model that leads to the wave-rotors proposed by De Leeuw [1986]. The evaporation of salt water will be treated in the way that was outlined previously by Mestayer [1990]. Salt water evaporation differs from fresh water, because the droplets can only shrink to a minimum size determined by their salt content and ambient relative humidity.

Chapter 3 presents our model for the mean air flow over the waves, which yields vertical profiles of U(z), W(z), $\rho_v(z)$ and T(z) in the non-evaporative and non-turbulent atmosphere. The movement of (sea spray) droplets in the non-turbulent air flow and in the absence of evaporation is discussed in chapter 4. In the budget equations of the SeaCluse model the terms that represent the fluxes of droplets due to their average movement are modelled by their vertical profiles that would be observed in the absence of turbulence and of evaporation.

During the actual run of the SeaCluse model, the atmosphere is turbulent and evaporation of droplets takes place. The algorithm for the evaporation of the salt water droplets is outlined in chapter 5, whereas chapter 6 discusses the implementation of the evaporation module in the Sea-Cluse code.

The results are briefly discussed in chapter 7, where we also indicate the line of work to further develop and test the SeaCluse model.

2 THE ORIGINAL CLUSE MODEL

The CLUSE model was developed by Rouault and Mestayer and has been extensively described [Rouault, 1989], [Rouault and Larsen, 1990], [Rouault et.al., 1991]. Therefore, only a compilation of the main hypotheses and model equations is given here.

The framework of the model is defined by the following hypotheses:

1. The fluid is incompressible
2. The Coriolis force is negligible
3. There are no chemical reactions
4. The Boussinesq approximation may be applied
5. The droplets are spherical and do not split
6. The number of droplets in the domain of study is conserved
7. The boundary layer is fully developed and the classical horizontal homogeneity hypothesis is applied. The constant flux hypothesis can be used in all the domain for the transportable variables that have no local source
8. The density of droplets is too small to have any influence on the dynamics of air
9. Only jet droplets are taken into account

The fluid is considered to be a multiphase mixture of N+2 components: dry air, with concentration ρ_a, water vapor with concentration ρ_v, and N droplet categories of radius r_n (n = 1..N) and concentration ρ_n. Category n includes all droplets of radius r defined by:[1]

$$r_n - \Delta r_n/2 < r \leq r_n + \Delta r_n/2 \qquad (2.1)$$

The instantaneous budget equation of mass of any of the N+2 transportable components is:

$$\frac{\partial \rho_\gamma}{\partial t} + \frac{\partial (\rho_\gamma V_{\gamma j})}{\partial x_j} = S_\gamma \qquad \begin{cases} \gamma = a, v, n \\ n = 1, \ldots, N \end{cases} \qquad (2.2)$$

1 See appendix A for a listing of all symbols used in this report

where $V_{\gamma j}$ is the velocity component in direction j of the component γ and S_γ is the net source term. In the CLUSE model, the exchange of mass between the components can only be due to droplet evaporation. Therefore:

$$\begin{cases} S_a = 0 \\ S_v + \sum_{n=1}^{N} S_n = 0 \end{cases} \tag{2.3}$$

The slip velocity is introduced as the velocity difference between a component and the local center of mass. We use the decomposition of a quantity Φ, which characterizes the turbulent flow, into a mean part $\bar{\Phi}$ and a fluctuating part Φ' such that $\Phi' = 0$. With this, and hypotheses 7 and 8, the instantaneous budget equations can be averaged to yield the mean budget equations:

$$\begin{cases} \underset{1}{\dfrac{\partial \overline{\rho_a}}{\partial t}} = 0 \\ \underset{1}{\dfrac{\partial \overline{\rho_n}}{\partial t}} = \underset{1}{-} \dfrac{\partial(\overline{\rho_n' w'})}{\partial z} \underset{2}{-} \dfrac{\partial(\overline{\rho_n' \Delta_{nz}'})}{\partial z} \underset{3}{-} \dfrac{\partial(\overline{\rho_n W_n})}{\partial z} \underset{4}{+} \underset{5}{S_n} \\ \underset{1}{\dfrac{\partial \overline{\rho_v}}{\partial t}} = \underset{1}{-} \dfrac{\partial(\overline{\rho_v' w'})}{\partial z} \underset{2}{-} \sum_{n=1}^{N} S_n \end{cases} \tag{2.4}$$

where W_n and Δ_{nz} are the vertical components of droplet mean and slip velocity, respectively, and w' denotes the fluctuating component of the vertical air flow. In addition, the budget equation of sensible heat can be written as:

$$\underset{1}{\rho_a c_{pa} \frac{\partial \overline{T}}{\partial t}} = \underset{2}{-\rho_a c_{pa} \frac{\partial(\overline{T' w'})}{\partial z}} + L_v \sum_{n=1}^{N} S_n \tag{2.5}$$

where c_{pa} and L_v denote the specific heat of air at constant pressure and the latent heat of evaporation, respectively.

Terms 1 in (2.4) and (2.5) denote the local time rates of changes. As its name implies, the CLUSE model calculates the stationary solution. Hence, terms 1 are zero at equilibrium.

Terms 2 in (2.4) and (2.5) represent the diffusion by the air turbulent movements and are modelled by means of exchange coefficients K_i. The coefficients K_i are equal for all droplet categories, water vapor and temperature and are given by the eddy viscosity σ_t:

$$\begin{cases} \overline{\rho_\gamma' w'} = - K \dfrac{\partial \overline{\rho_\gamma}}{\partial z} & \gamma = n, v \\ \overline{T' w'} = - K \dfrac{\partial \overline{T}}{\partial z} & \\ K = \sigma_t \; / \; 0.74 & \end{cases} \tag{2.6}$$

where the factor 0.74 represents the turbulence Schmidt (water vapor, droplets) or Prandtl (temperature) numbers that are all equal (see also [Melville and Bray, 1979]).

Term 3 in (2.4) denotes the counterdiffusion, which appears because the droplets do not exactly follow the turbulent motions of the air due to their inertia. Term 3 reduces the turbulent diffusion as a function of droplet radius and turbulence intensity. It is modelled by an exchange coefficient K_n':

$$\begin{cases} \overline{\rho_n' \Delta_{nz}'} = - K_n' \dfrac{\partial \overline{\rho_n}}{\partial z} & \\ K_n' = -K_n \left[1 - \dfrac{1}{1 + C_2 \; (V_{f,n}^2 \; / \; 1.56 u_*^2)} \right] & \end{cases} \tag{2.7}$$

where V_f and u_* denote final fall velocity and friction velocity, respectively. The constant C_2 is one of the two model tune parameters to be adjusted by comparison with experimental data.

Term 4 in (2.4) governs the macroscopic fluxes due to ejection of droplets from the surface and their gravitational fall. Rouault et.al. [1991] proposed to model this term by:

$$\frac{\partial(\overline{\rho_n W_n})}{\partial z} = \frac{1}{C_1 T_{fly,n}} \left[\overline{\rho_n}(z) - \rho_n^0(z) \right] \qquad (2.8)$$

where T_{fly} denotes the flight time of the droplets and ρ_n^0 the concentration in non-turbulent and non-evaporative conditions. The constant C_1 is the other model tune parameter to be adjusted by comparison with experimental data.

Finally, term 5 in (2.4) represents the source terms due to droplet evaporation. Within the hypothesis of conservation of the total number of droplets, Mestayer and Lefauconnier [1988] formulated a model that yields an expression for S_n:

$$S_n = 6 \rho_n \frac{\dot{r}_n}{r_n} - \dot{r}_n \frac{\partial \rho_n}{\partial r_n} - \rho_n \frac{\partial \dot{r}_n}{\partial r_n} \qquad (2.9)$$

In the CLUSE model for fresh water the rate of change of droplet mass $\dot{r}$ is described by Beard and Pruppacher's [1971] model of an evaporating droplet falling at terminal velocity, which also gives good results for evaporating droplets in a turbulent flow [Edson, 1989].

When we substitute (2.6)-(2.8) in (2.4) and (2.5), the set of CLUSE equations is closed. The CLUSE equations all have the same general form:

$$\begin{cases} \dfrac{\partial \overline{\Phi}}{\partial t} = \dfrac{\partial}{\partial z}\left(K \dfrac{\partial \overline{\Phi}}{\partial z}\right) + S_\Phi = 0 \\ S_\Phi = S_U + \Phi S_P \end{cases} \qquad (2.10)$$

where S_Φ includes every term but turbulent diffusion and inertia counterdiffusion. The solution, i.e., the time limit of the non-stationary equation, is found by an iterative process. The equations are discretised by the finite volume method [Patankar and Spalding, 1970] and subsequently solved with a tridiagonal algorithm [Schiestel, 1991].

Initial and boundary conditions are needed to solve the equations. For water vapor and temperature these have been defined as:

$$
\begin{cases}
\textit{Initial:} & \text{Logarithmic profiles} \\
\textit{Upper boundary:} & \overline{T}(z_{max}) = T(z_{max}) \qquad \overline{\rho_v}(z_{max}) = \rho_v(z_{max}) \\
\textit{Lower boundary:} & \overline{T}(z_{min}) = T_{surf} \qquad \overline{\rho_v}(z_{min}) = \rho_{vs}(T_{surf})
\end{cases}
$$

where ρ_{vs} denotes the saturated water vapor concentration. For the droplets these conditions are:

$$
\begin{cases}
\textit{Initial:} & \overline{\rho_n}(z) = 0 \\
\textit{Upper boundary:} & \overline{\rho_n}(z_{max}) = 0 \quad \textit{and} \quad \dfrac{\partial \overline{\rho_n}(z_{max})}{\partial z} = 0 \\
\textit{Lower boundary:} & \overline{\rho_n}(z_{min}) = \rho_{ej,n} - \dfrac{\int_{z_{min}}^{z_{max}} S_n dz + \rho_{ej,n} V_{up,n}}{V_{f,n}}
\end{cases}
$$

where ρ_{ej} and V_{up} denote the concentration of ejected droplets and the ejection velocity, respectively. The boundary conditions result from the constraint that the total number of droplets throughout the domain is conserved. At the lower boundary, the concentration of droplets is the sum of the concentrations of droplets ejected from the sea and falling back into the sea.

3 MODEL FOR THE AIR FLOW OVER THE WAVES

3.1 Visualization of the calculation

In this chapter we discuss our 2-dimensional model of the air flow over the waves (height and one horizontal coordinate). The model will be used to calculate the trajectories of sea spray droplets and subsequently, the vertical concentration profiles of the droplets.

It is important to keep in mind that the SeaCluse model is an 1-dimensional Eulerian model (height only) and that it does not deal with the coordinates x and y. This can be visualized by an observer who remains fixed at a certain position x and watches the waves go by. The waves induce changes in the values of U(z), T(z), $\rho_v(z)$, etc. Since the model calculates a stationary solution, the observer cannot specify these variables as a function of time. Therefore, they have to be averaged over the waves, i.e., to be averaged over a time $t >> \omega^{-1}$, where ω is the wave period.

In our model, variables like U(z) vary periodically in time with ω and it suffices to average over $t = \omega^{-1}$. This is most conveniently done in a coordinate system that moves along with the wave (with the phase velocity C_p). In such a system, the position of the wave surface does not move, or, $\eta(x,t) = \eta(x)$. The integration (averaging) in time mentioned above is then replaced by an integration in space (over the wave surface).

3.2 Basic parameters

Our aim was to develop a model that only requires input parameters that are readily available, such as wind speed and temperature. As a result, the key input parameter for the model is U_{10}, i.e., the wind speed at a reference height of 10 meters. In our model, U_{10} directly determines the amplitude and frequency of the wave, as well as the friction velocity. The latter parameter plays an important role in the calculation of the vertical profiles of U, W, ρ_v and T, as we will see later.

The friction velocity u_* is calculated from U_{10} and the drag coefficient C_{DN}:

$$u_*^2 = C_{DN} U_{10}^2 \qquad (3.1)$$

The value of the drag coefficient has been measured by many authors (see [Geernaert, 1990] for an overview) and depends on U_{10}, wave state and region. We use values for open ocean (North Atlantic) and coastal regions (Meetpost Noordwijk) as given by [Smith, 1980] and [Davidson et al., 1993], respectively:

$$\begin{cases} 10^3\, C_{DN} = 0.61 + 0.063\, U_{10} & \text{open ocean} \\ 10^3\, C_{DN} = 0.43 + 0.100\, U_{10} & \text{Meetpost Noordwijk} \end{cases} \tag{3.2}$$

For the first version of the SeaCluse model, we have chosen a simple wave model. We assume that the waves can be described by a first order Stokes wave:

$$\eta(x,t) = -\frac{1}{2}H_0 \cos(kx-\omega t) + \frac{1}{8}H_0 k \cos(2kx-2\omega t) \tag{3.3}$$

where the wave amplitude H_0 and frequency ω are given by [Edson, 1990]:

$$\omega = \frac{g}{\Gamma_1 U_{10}} \qquad H_0 = \frac{\pi\, \Gamma_1^2\, U_{10}^2}{10g} \tag{3.4}$$

The factor Γ_1 in (3.4) is the wave age parameter, which in our model is fixed at $\Gamma_1 = 0.7$, i.e, the value for fully developed waves. Obviously, the assumption of fully developed waves will often be violated in coastal regions (see, e.g., [Maat et al., 1991]).

3.3 The eddy diffusivity

The eddy diffusivity is an important parameter, since it governs the diffusion of heat, moisture and droplets by the air turbulent movements in the CLUSE model (see equation (2.6)). In addition, the eddy diffusivity appears indirectly in (2.7) for the counterdiffusion due to droplet inertia.

To calculate the eddy diffusivity, we divided the vertical axis in two regions:

(a) The wave region, where the waves influence the air flow.
(b) The atmospheric region, where the waves no longer influence the air flow.

In the atmospheric region, we apply the condition of a fully developed boundary layer (classical atmospheric surface layer). In that case, the eddy diffusivity σ_t is given by:

$$\sigma_t(z) = \kappa u_* z \qquad z > H_0 \tag{3.5}$$

In the wave region, we assume that momentum is only transferred to the water and not to the waves. We also assume that the structure of the mean flow is locally that of a turbulent boundary layer over a flat surface. In that case, local profiles $\sigma_t(x,z)$ may be calculated by:

$$\begin{cases} \sigma_t(x,z) = \kappa u_* (z - \eta(x)) & \eta(x) < z < H_0 \\ \sigma_t(x,z) = 0 & -\frac{1}{2}H_0 < z \leq \eta(x) \end{cases} \tag{3.6}$$

where $\eta(x)$ corresponds to the height of the wave surface at position x. Note that $\eta(x)$ is not a function of time, since we perform the calculation in the coordinate system that moves along with the waves. The average profile $\sigma_t(z)$ in the wave region is calculated by:

$$\sigma_t(z) = \int_0^{\lambda/2} \sigma_t(x,z)\, dx \qquad -\frac{1}{2}H_0 < z < H_0 \tag{3.7}$$

where it suffices to integrate over half a wave period, i.e., from trough to crest, due to symmetry.[2]

It has been reported that the wave region, where the waves influence the air flow, extends up to 5-10 times H_0 (the wave crest is at $z \approx \frac{1}{2}H_0$). However, when constructing the profile of σ_t by (3.5) and (3.6), we found that there was no difference between the average of the local profiles and the 'atmospheric' σ_t above $z = H_0$. Figure 3.1 shows the resulting profile of $\sigma_t(z)$. The net effect of the wave surface integration is that the slope of $\sigma_t(z)$ is decreased and consequently, $\sigma_t(z) = 0$ is

2 In general, the integration is not straightforward because the $\sigma_t(x,z)$ profiles have to be averaged over the wave surface. This requires a grid that is equidistantly spaced over the wave surface, which is not the same as a grid equidistantly spaced in x. In appendix B we show that the error by replacing the wave grid by an x-grid is negligible in the case that the waves are modeled by a Stokes wave.

reached below z = 0. The number of local profiles that are averaged is not very important. A minimum of 20 is required; averaging 500 profiles yields essentially the same results.[3]

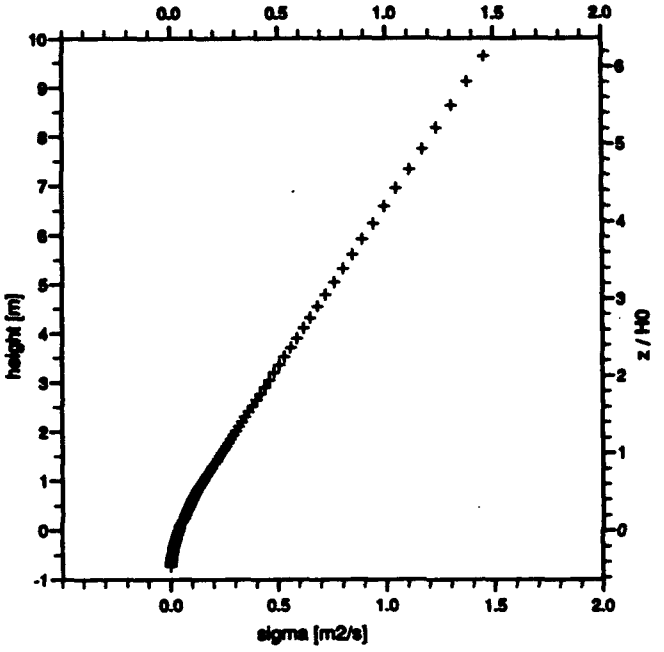

Figure 3.1: Vertical profile of eddy diffusivity in the lower region of the calculation domain

3.4 The profile of horizontal wind speed

With the hypothesis that the constant flux assumption is valid for momentum in the atmospheric region, the wind profile may be calculated from $\sigma_t(z)$ by:

$$\frac{\partial U}{\partial z} = \frac{u_*^2}{\sigma_t} \phi_m \qquad z > H_0 \qquad (3.8)$$

where ϕ_m denotes the atmospheric stability function (see, e.g., [Edson et al., 1991]). In neutral stratification $\phi_m = 1$; for non-neutral conditions, the Monin-Obhukov length L is needed to

3 Appendix C discusses another method to calculate σ_t, based on the assumption of a fully developed and dominant wave rotor. However, with this method it was not possible to construct reliable profiles of U, ρ_v and T. Interestingly, the method of 'local profiles' discussed in the text finally leads to a wave rotor too (see below).

calculate ϕ_m. Because z_{0u}, T_* and ρ_{v*} are not yet available, it is not straightforward to obtain L. Therefore, SeaCluse is developed first for neutral conditions.

Equation (3.8) shows that a reference value for U is needed to construct the profile. For this, we take the value of the input variable U_{10} at z = 10 m. From there, the wind profile is constructed to the top of the boundary layer and down to $z = H_0$.

The wind profile thus obtained can be used to infer another important parameter for the modelling of turbulence: the roughness length z_{0u}. To this end, linear regression is applied to fit the wind profile to:

$$U(z) = \frac{u_*}{\kappa} \ln\left(\frac{z}{z_{0u}}\right) \qquad z > H_0 \tag{3.9}$$

which yields a value for z_{0u}. We may compare the value of z_{0u} with values for the roughness length z_0 obtained by Charnock's relation or the Kitaigorodski model (see appendix D). Up to now, we have observed that z_{0u} is nearly equal to z_0.

The wind profile in the wave region is calculated in the moving coordinate system, where $\eta(x,t) = \eta(x)$. In that case, local logarithmic profiles U(x,z) are given by:

$$U(x,z) - u_{0L}(x) = \frac{u_*}{\kappa} \ln\left\{\frac{z - \eta(x) + z_{0L}(x)}{z_{0L}(x)}\right\} \qquad \eta(x) \le z < H_0 \tag{3.10}$$

where $u_{0L}(x)$ denotes the local value of U(x,z) at the wave surface and $z_{0L}(x)$ represents the 'local' roughness length. It is easily verified that $u_{0L}(x) = U(x,\eta(x))$ when $z = \eta(x)$. The wind speed at the surface is composed of a local component due to the water orbital movement under the wave and a constant component due to surface slip:

$$U(x,\eta(x)) = \omega\eta(x) + \kappa u_* \tag{3.11}$$

where ω is the frequency of the Stokes wave. Subsequently, we apply the condition that all local profiles U(x,z) must converge to the value of U_{10} at z = 10 m, i.e., outside the wave region. Imposing this condition, $z_{0L}(x)$ can be calculated by:

$$U_{10} - u_{0L}(x) = \frac{u_*}{\kappa} \ln\left\{\frac{10 - \eta(x) + z_{0L}(x)}{z_{0L}(x)}\right\} \qquad (3.12)$$

Finally, the average profile U(z) in the wave region is calculated by:

$$U(z) = \int_0^{\lambda/2} U(x,z)\, dx \qquad -\frac{1}{2}H_0 < z < H_0 \qquad (3.13)$$

where dx runs over half a wave period, i.e., from trough to crest. The number of local profiles should be fairly large (≈ 500) to obtain a smooth wind profile in the wave region. Figures 3.2a-c show $\eta(x)$, $u_{0L}(x)$ and $z_{0L}(x)$ for U_{10} = 10 m/s. The largest values of u_{0L} and z_{0L} are found at the crest. Note that the mean value of u_{0L} is slightly larger than κu_*, due to the asymmetry of the Stokes wave.[4]

Finally, figure 3.3 shows the complete wind profile U(z) for U_{10} = 10 m/s. A nearly perfect match is observed at the intersection of the atmospheric and wave regions at z = H_0.

---

4 The second term in (3.3) causes the wave trough and crest to be located at z = -0.46 H_0 and z = 0.53 H_0, respectively, rather than at z = ± ½H_0

a)

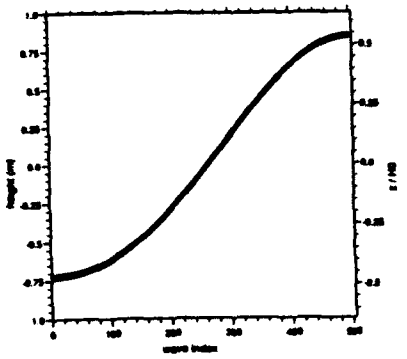

c)

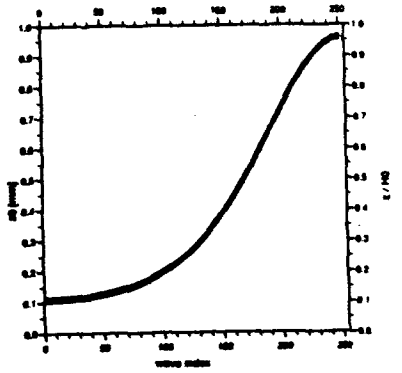

b)

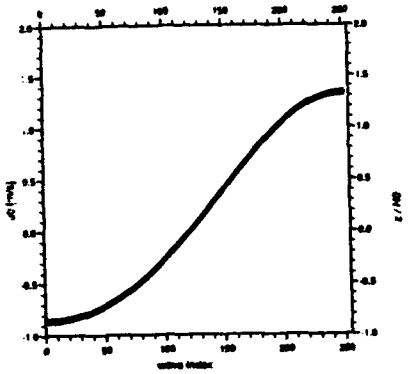

Figure 3.2: Parameters of the local wind profiles
a) Height of the wave surface $\eta(x)$ as a function of x;
b) Surface value $U(x,\eta(x))$ or $u_{QL}(x)$ as a function of x;
c) Local roughness length $z_{QL}(x)$ as a function of x;

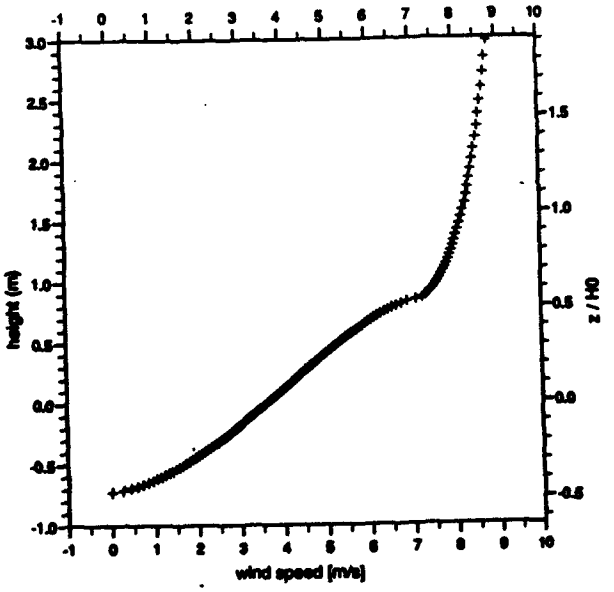

Figure 3.3: Average wind profile U(z) as a function of height

3.5 The temperature profile

The initial profile of temperature is calculated in almost the same manner as the wind profile. Thus, in the atmospheric region, where the constant flux assumption is valid in the absence of evaporating droplets, $\sigma_t(z)$ is used to calculate T(z):

$$\frac{\partial T}{\partial z} = \frac{u_* T_* Pr_t}{\sigma_t} \qquad (z > H_0) \tag{3.14}$$

where the Prandtl number $Pr_t = 0.74$ [Rouault et.al., 1991]. The model input parameter T_{10} (temperature at 10 m AMSL) serves as the reference value needed to calculate the profile. The scaling factor T_* is inferred from:

$$T_* = \frac{C_H}{u_*} (U_{10} - \kappa u_*) (T_{10} - T_{surf}) \tag{3.15}$$

where we use the average value $C_H = 0.001$.

The temperature profile in the wave region is again calculated in the moving coordinate system, from local logarithmic profiles T(x,z):

$$T(x,z) - T_{surf} = \frac{Pr_t T_*}{\kappa} \ln\left\{\frac{z - \eta(x) + z_{0L}(x)}{z_{0L}(x)}\right\} \qquad \eta(x) \le z < H_0 \tag{3.16}$$

where we assume that the surface temperature does not vary over the wave. The local temperature roughness length $z_{0L}(x)$ does depend on x and is again found by imposing the condition that all local profiles converge to T_{10} at z = 10 m:

$$T_{10} - T_{surf} = \frac{Pr_t T_*}{\kappa} \ln\left\{\frac{10 - \eta(x) + z_{0L}(x)}{z_{0L}(x)}\right\} \tag{3.17}$$

The average profile T(z) in the wave region is calculated by integrating the local profiles over the wave surface. Just as in the case of the wind profile, the number of local profiles should be circa

500. Figure 3.4 shows the temperature profile for T_{10} = 20 °C and T_{surf} = 10 °C (and U_{10} = 10 m/s). Note that the atmospheric profile and the wave region profile match perfectly at the intersection ($z = H_0$).

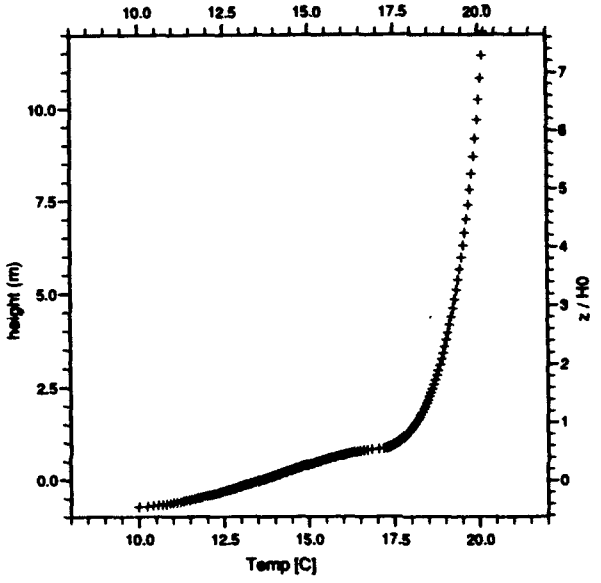

Figure 3.4: Profile of temperature as a function of height

3.6 The humidity profile

The humidity profile of humidity is calculated in exactly the same manner as the temperature profile. Thus, for the atmospheric region:

$$\frac{\partial \rho_v}{\partial z} = \frac{u_* \, \rho_{v*} \, Sc_t}{\sigma_t} \qquad (z > H_0) \qquad (3.18)$$

where the Schmidt number Sc_t = 0.74 [Rouault et.al., 1991]. The scaling factor ρ_{v*} is calculated from:

$$\rho_{v*} = \frac{C_E}{u_*} (U_{10} - \kappa u_*) (\rho_{v,10} - \rho_{v,0}) \qquad (3.19)$$

where we use the average value $C_E = 0.0012$. The values for $\rho_{v,10}$ and $\rho_{v,0}$ are obtained from conversion of the input parameter RH_{10} and the relative humidity at the sea surface (RH = 97%, determined by the salinity), respectively.

In the wave region, local logarithmic profiles $\rho_v(x,z)$ are calculated with $\rho_{v,0} = RH_{surf}$ and a local roughness length $z_{0L}(x)$ inferred from $\rho_{v,10}$ by expressions analogous to (3.16) and (3.17). The average profile $\rho_v(z)$ is calculated by an integration over circa 500 local profiles (cfr (3.13)).

An example of the resulting overall profile of humidity is shown in figure 3.5, for $RH_{10} = 75\%$ (and $U_{10} = 10$ m/s, $T_{10} = 20$ °C, $T_0 = 10$ °C). For convenience, the profile is given as a relative humidity profile.

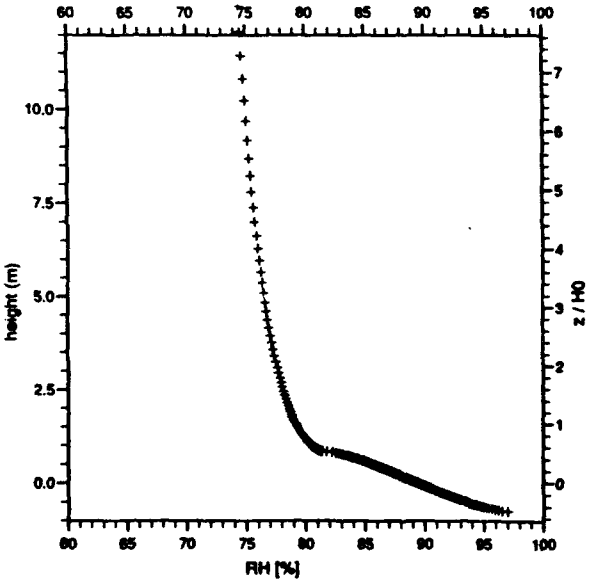

Figure 3.5: Profile of relative humidity as a function of height

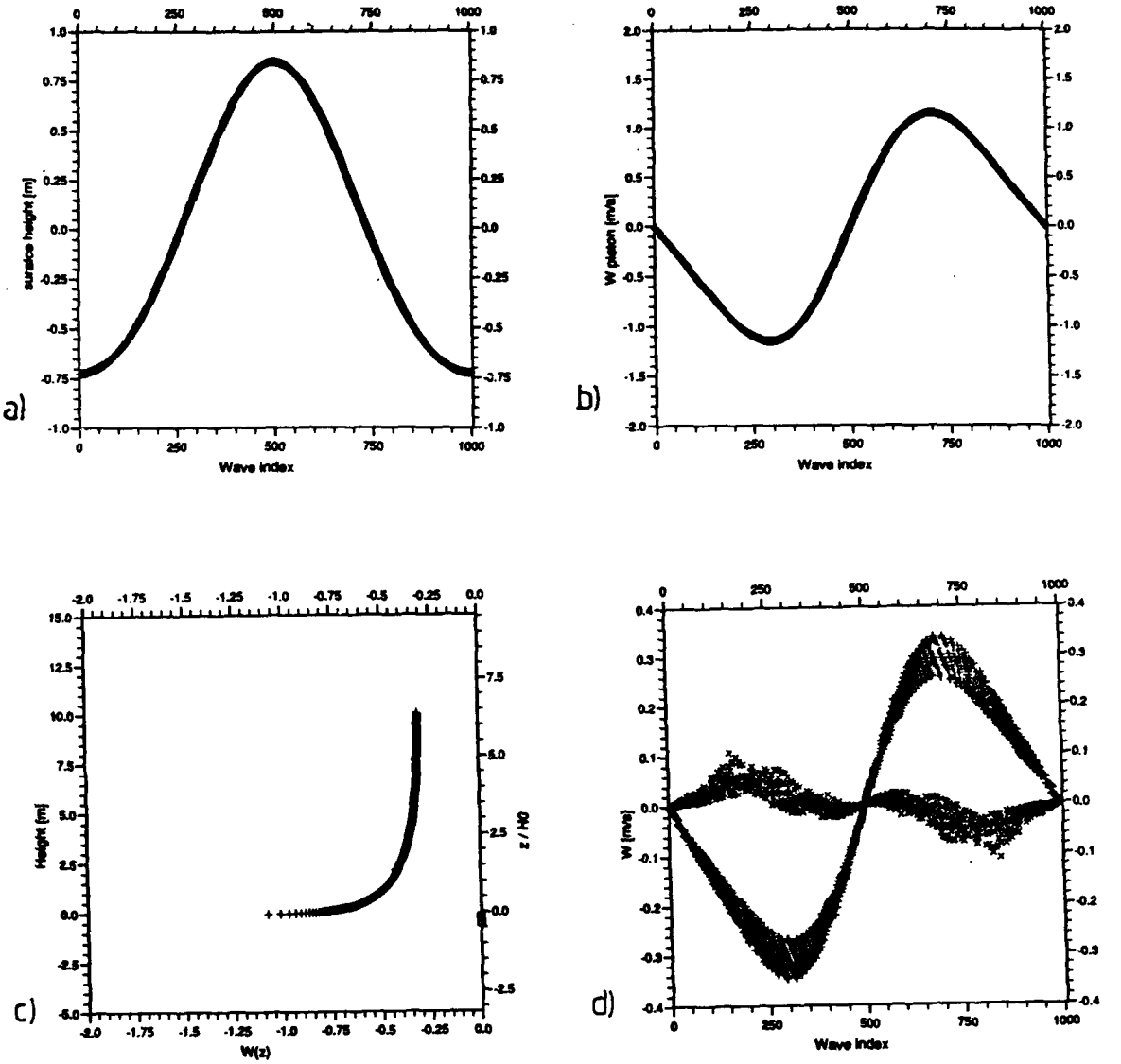

Figure 3.6: Parameters for the wind field W(x,z)
a) Height of wave surface versus x-grid index
b) Piston velocity versus x-grid index
c) Example of local profile of vertical wind component
d) Vertical wind component distribution over the wave at 10 m (see text)

Figure 3.6 shows results for a calculation of W(x,z). In this specific case, U_{10} = 10 m/s and 1000 local U-profiles were used (x-grid density). The wave travels in the +x direction and the z-grid has Nz grid points between z = -½H_0 and z = 10 mtr. Figures 3.6a and 3.6b show the height of the wave surface $\eta(x)$ and the piston velocity as a function of x-grid index, respectively. Figure 3.6c shows a local wind profile W(x,z) at the windward side of the wave (i.e., wave surface moving down), obtained with Nz=1000.

The success of the calculation of the local profiles W(x,z) may be verified in the region well above the waves, where the waves no longer have any influence on W(x,z). Thus, in that region W(x,z) should be independent of x. Figure 3.6d shows W(x,z) at a height of 10 mtr (≈ 6.5 H_0 for U_{10}=10 m/s) as a function of x. It was constructed by taking the value W(x,z=10) of each of the local profiles W(x,z). The curve marked by (+) was obtained from local profiles W(x,z) that had been calculated with 1000 vertical grid points between the surface and 10 m AMSL, the curve marked by (x) from local profiles W(x,z) that had 10000 vertical grid points. It is easily seen from figure 3.6d that Nz should be in the order of 10^4 to obtain a wind field W(x,z) that is independent of x above the wave region.

Since both U(x,z) and W(x,z) are now determined, a vector plot of the wind field over the wave can be constructed. Such a plot is shown in figure 3.7, where the length and direction of the arrows represent wind speed and wind direction, respectively. Our model for the air flow over the waves results in a perfectly symmetric wind field with a rotor between the wave crests. The influence of the waves decreases with height and becomes negligible above 2-3H_0.

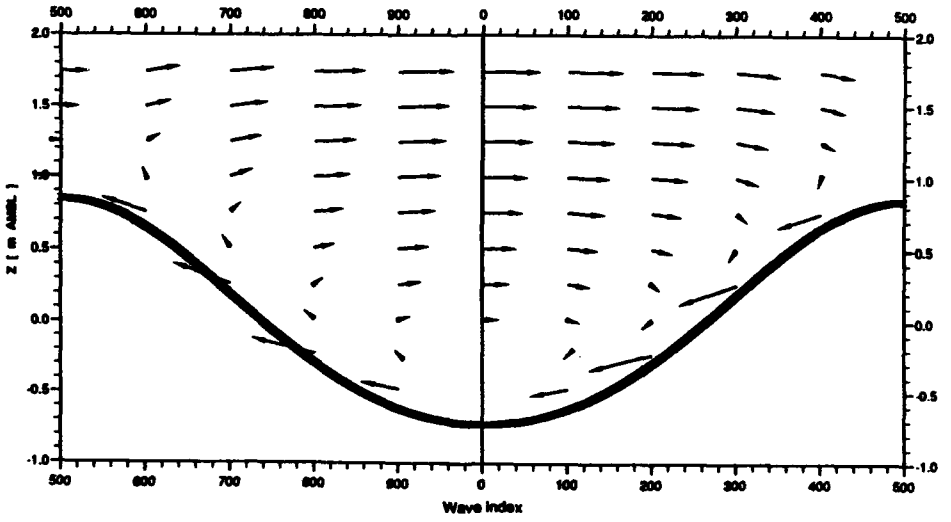

Figure 3.7: Air flow over the wave

4 DROPLET MOVEMENT IN THE AIR FLOW

4.1 Ejection height and ejection velocity

In order to calculate the trajectories of the sea spray droplets that result from bursting bubbles, we need to know their ejection velocities $V_{up}(D)$. To this end, we first infer the ejection heights $H_{ej}(D)$ of the droplets from Blanchard's ejection data [Blanchard, 1963, 1989] for jet droplets consisting of distilled water of 22-26 °C. Blanchard's figures show negligible difference between distilled water and seawater. Subsequently, ejection velocities $V_{up}(D)$ are calculated from $H_{ej}(D)$ by an iterative procedure described previously [Wu, 1979; Rouault et.al., 1991]. The method uses the equation of vertical motion in non-turbulent and non-evaporative conditions over a horizontal still surface (see below, (4.2)) and an initial guess for $V_{up}(D)$ to infer the maximum height H(D) that the droplet reaches. The value for $V_{up}(D)$ is then gradually adjusted untill $H(D) = H_{ej}(D)$.

4.2 Droplet trajectories

The presence of waves complicates the calculation of the droplet trajectories, because the horizontal displacement of the droplet and the movement of the air itself must also be taken into account. The trajectories are most conveniently calculated in the coordinate system that moves along with the waves (phase velocity C_s). In this system, the horizontal and vertical droplet velocities u_d and w_d are given by:

$$\begin{cases} u_d(D,x,z,t) = u_r(D,t) + U(x,z) - C_s \\ w_d(D,x,z,t) = w_r(D,t) + W(x,z) \end{cases} \tag{4.1}$$

where U(x,z) and W(x,z) are the local horizontal and vertical wind speed (see §3.4 and §3.7) and $u_r(D,t)$ and $w_r(D,t)$ denote the horizontal and vertical velocity of the droplet relative to the air:

$$\begin{cases} \dfrac{\partial u_r}{\partial t} = -\dfrac{3}{4} C_D \dfrac{\rho_a}{\rho_w} \dfrac{u_r|u_r|}{D} \\ \dfrac{\partial w_r}{\partial t} = -\dfrac{3}{4} C_D \dfrac{\rho_a}{\rho_w} \dfrac{w_r|w_r|}{D} - g \end{cases} \tag{4.2}$$

In (4.2), C_D denotes the drag coefficient; for a spherical droplet C_D is a function of the Reynolds number Re:

$$\mathrm{Re} = \sqrt{u_r^2 + w_r^2}\,\frac{D}{\nu} \tag{4.3}$$

where ν is the kinematic viscosity of air. The drag coefficient is calculated by [Raudviki, 1979]:

$$\begin{cases} C_D = 24 \,/\, \mathrm{Re} & \mathrm{Re} < 0.5 \\ C_D = 24\,(1 + 0.19\mathrm{Re}) \,/\, \mathrm{Re} & 0.5 \le \mathrm{Re} < 2 \\ C_D = 24\,(1 + 0.15\mathrm{Re}^{0.687}) \,/\, \mathrm{Re} & 2 \le \mathrm{Re} \end{cases} \tag{4.4}$$

The initial velocities $u_r(D,t=0)$ and $w_r(D,t=0)$ needed to calculate $u_r(D,t)$ and $w_r(D,t)$ by (4.2) are given by:

$$\begin{cases} u_r(D,t=0) = U(x_{ej}, \eta(x_{ej})) = u_{0L}(x_{ej}) \\ w_r(D,t=0) = V_{up}(D) \end{cases} \tag{4.5}$$

Note that the initial velocity $u_r(D,t=0)$ depends on the position over the wave surface where the droplet is ejected (and is equal to the horizontal component of the air flow at the surface).

Equations (4.1)-(4.5) allow the calculation of the trajectory of a droplet ejected at $x = x_{ej}$. The calculation is aborted when the droplet hits the water surface, i.e., when:

$$z_d \le \eta(x_d) \tag{4.6}$$

The calculation is most effectively done in a grid that is equidistantly spaced along the droplet trajectory.[5] Such a grid with step-size $\delta p(D)$ is built by recalculating Δt in each cycle:

$$\Delta t(D,x,z,t) = \frac{\delta p(D)}{\sqrt{u_d(D,x,z,t)^2 + w_d(D,x,z,t)^2}} \tag{4.7}$$

---

5 The trajectory can also be calculated in the more common manner, that is, with a constant Δt (typically, $\Delta t = 50$ μs is needed), but in that case 5-10 times as many steps are required to obtain the same accuracy.

The time step Δt is small when the velocity of the droplet with respect to the wave surface is high,[6] whereas it becomes larger when the droplet slows down. The step size $\delta p(D)$ depends on the size of the droplet, and varies between 0.02-0.5 cm for $20 \leq D \leq 500$ μm.

An example of a typical trajectory is shown in figure 4.1a. In this case, $U_{10} = 10$ m/s, the wave is travelling in the +x direction and a droplet with a diameter of 10 μm was ejected from the wave trough. It is emphasized that this trajectory is calculated in a non-turbulent and non-evaporative atmosphere.

Different trajectories are obtained when droplets ($D \leq 110$ μm) are ejected from the lee side of the wave. They do not simply fall back, but are lifted upwards and enter in the wave rotor (figure 3.7). In some cases, they return to the surface (see figure 4.1b), but in other cases they start to move in a circle (see figure 4.1c).

6 This means that the relative velocity (u_r, w_r) of the droplet is high, and/or the droplet is at a position (x,z) where the wind field (U,W) is strong.

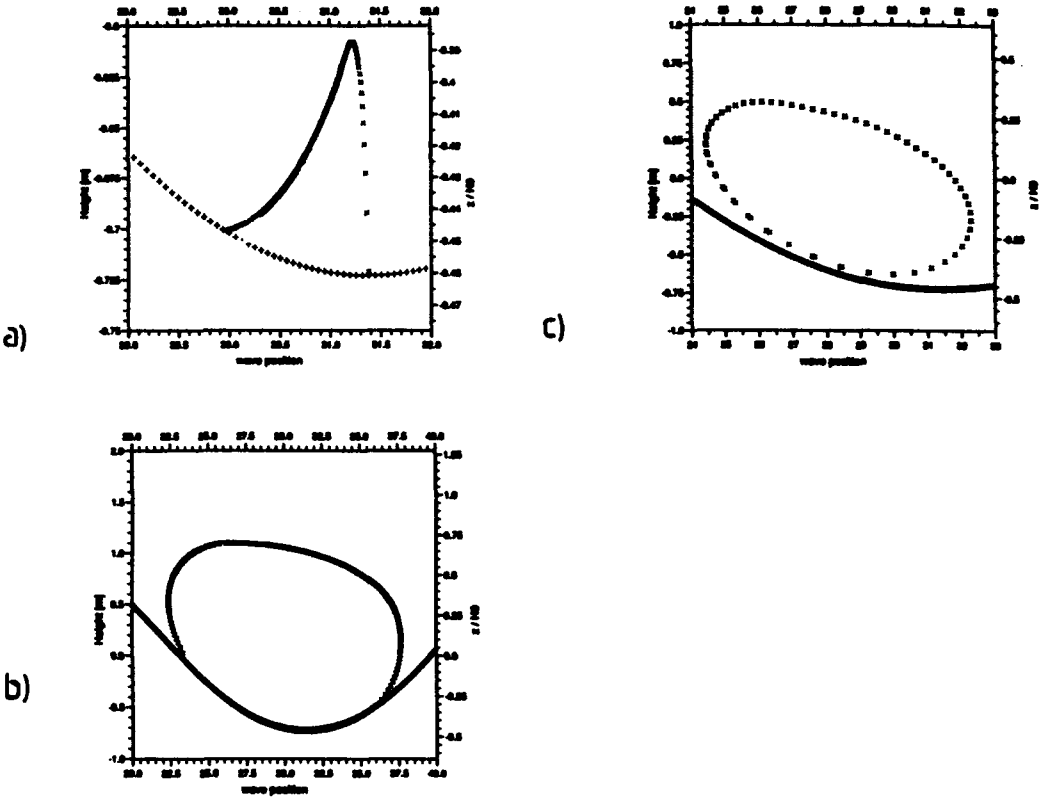

Figure 4.1: Representative droplet trajectories
a) Trajectory not influenced by the wave rotor
b) Trajectory entering the wave rotor
c) Circular trajectory

Clearly, the criterium that the trajectory calculation is finished when the droplet hits the surface again, will not work for droplets moving in a closed trajectory. In our opinion, the circular trajectories are an artefact resulting from the perfect symmetry of our model of the air flow over the waves. In reality, the wave surface is not perfectly smooth. Small variations in $\eta(x)$ induce asymmetry in the wave rotor with the consequence that the droplets do not move indefinitively in a perfect circle. Therefore, we decided to stop the calculation of circular trajectories after a full circle,[7] with the simultaneous removal of the droplets from the atmosphere.

4.3 Flight time

The suspension or flight time $T_{fly}(x,D)$ of the droplet is the sum of all time intervals Δt of the trajectory calculation. A plot of $T_{fly}(x,D)$ as a function of the position x where the droplet was ejected, is shown in figure 4.2a. In this case, U_{10}=10 m/s, D=500 μm, x=1 and x=51 correspond to

7 More precisely, the calculation is aborted when the droplet has passed $x = x_{sj}$ for the second time and starts to move away from the wave surface.

wave trough and crest respectively, and the wave is travelling in the +x direction. The flight time is larger at the lee side of the wave (x > 51, surface moves up) due to the airflow that moves the air upwards. The opposite effect is observed at the windward side of the wave, where the air moves down and shortens the flight time.

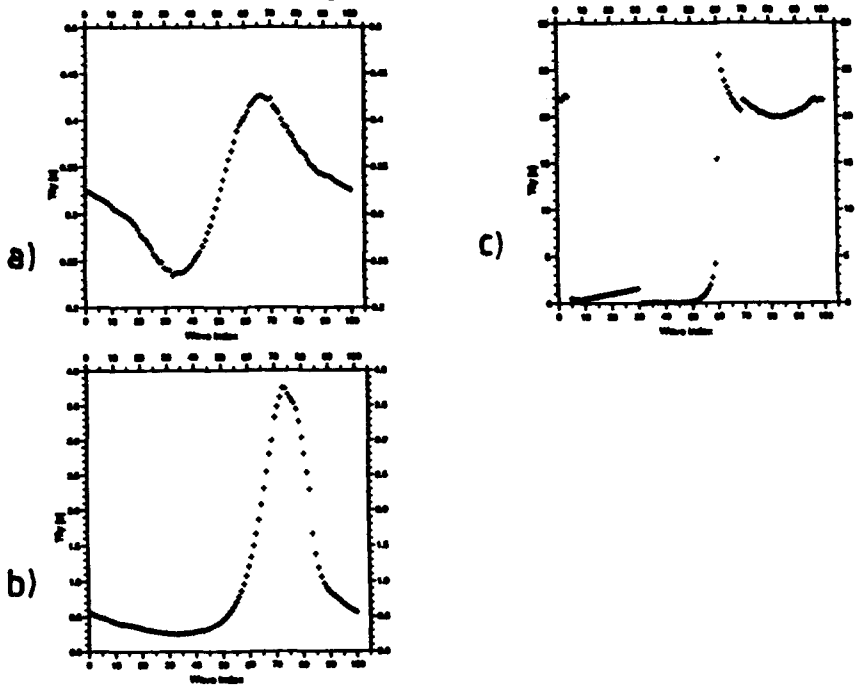

Figure 4.2: Flight times T_{fly} over the wave (see text for explanation of discontinuities)
a) T_{fly} for droplets of D=500 μm
b) T_{fly} for droplets of D=120 μm
c) T_{fly} for droplets of D= 20 μm

Figure 4.2b shows $T_{fly}(x,D)$ as a function of x for a droplet of D=120 μm. In this case, the prolongation of the flight time at the lee side of the wave is much larger than the shortening at the weather side. This reflects the facts that the droplets ejected at the weather side enter the wave rotor and complete a semi-circular trajectory (see figure 4.1b).

As the diameter of the droplet decreases, the prolongation of the flight time becomes larger and larger. Figure 4.2c shows $T_{fly}(x,D)$ for droplets of D=20 μm. The general shape of the curve in fig.4.2c can be explained in terms of the wave rotor, but there are also two artificial discontinuities in fig.4.2c (at x=30 and x=68) due to the discretization of the trajectory calculation.

The x-dependency of $T_{fly}(x,D)$ is removed in the integration over the wave surface:

$$T_{fly}(D) = \int_0^{\lambda} T_{fly}(x,D)\ dx \tag{4.8}$$

A plot of $T_{fly}(D)$ versus D is shown in figure 4.3 (curve marked by (+)), where we also present $T_{fly}(D)$ for the case of a flat surface (curve marked by (x)). It is easily seen that the presence of waves has little influence on the flight time of the large and heavy droplets that fall down quickly due to gravitation, but has a large effect on the flight times of the small and light droplets that may enter the wave rotor and start to move in a circle.

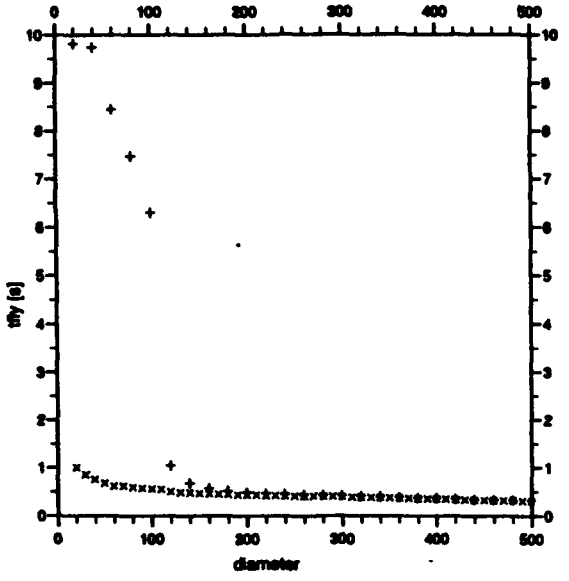

Figure 4.3: Average flight times for droplets over the waves (+) and over a flat surface (x)

The number of x-grid points over the wave (Nx) needed to obtain the average flight time $T_{fly}(D)$ ranges from only 20 in the case of large droplets to 50 for droplets that may enter the wave rotor ($D < 100\ \mu m$). In fact, a further increase of Nx does not yield more reliable average flight times, because the individual flight times $T_{fly}(x,D)$ are basically divided in 'long' and 'short' flight times (see figure 4.2c).

4.4 Final fall velocities

The plots of $V_f(x,D)$ versus x are less complicated, since all except the largest droplets reach their final fall velocity at a rather early stage of their trajectory. Therefore, $V_f(x,D)$ is only dependent on x for the largest droplets (see figure 4.4 for a plot of $V_f(x,D)$ versus x for droplets of D=500 μm). Not surprisingly, the larger values for $V_f(x,D)$ are found at the lee side of the wave where the flight times are longer.

Figure 4.5 shows the average final fall velocities $V_f(D)$ versus D after integration over the wave surface (+) (Nx as for the flight times, see above). For comparison, the fall velocities in the case of a flat surface are also plotted (x). The two curves are nearly identical.

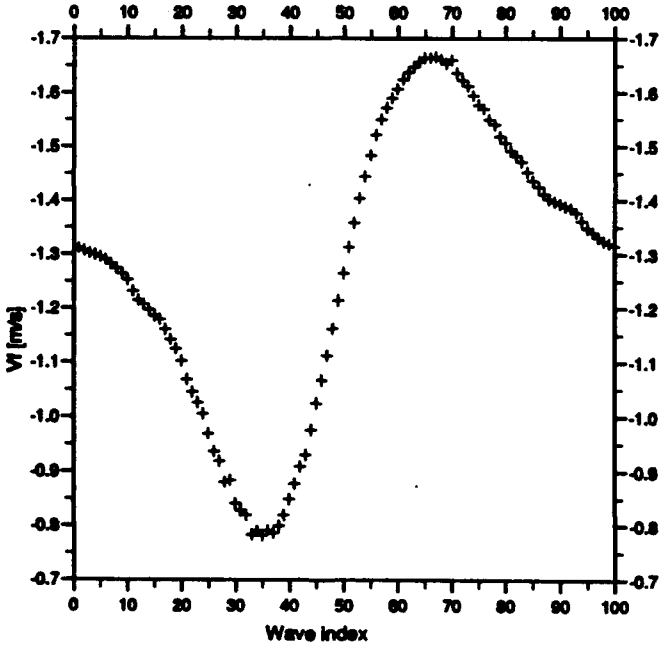

Figure 4.4: Final fall velocities V_f over the wave for droplets of D=500 μm

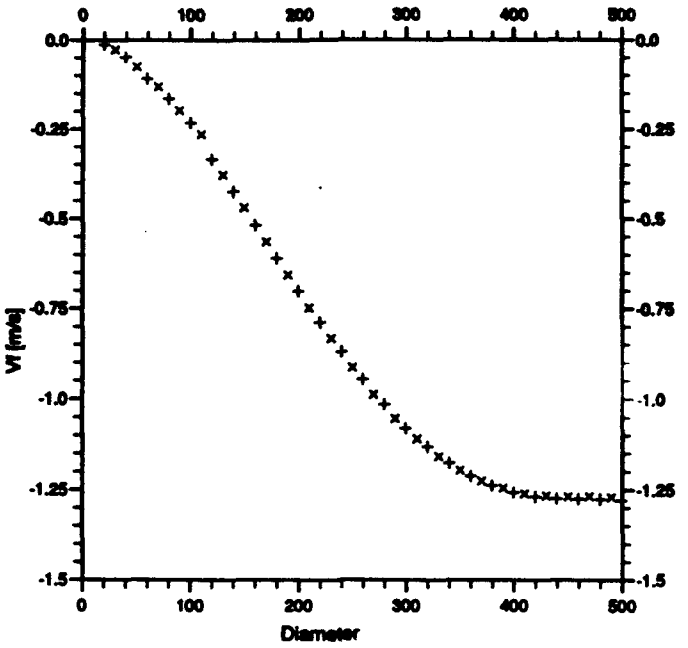

Figure 4.5: Average final fall velocities for droplets over the waves (+) and over a flat surface (x)

4.5 Profiles of droplet concentration

The last and most complicated of the droplet parameters is the vertical profile of droplet concentration. This profile is calculated with our model of the airflow over the waves, and therefore represents non-turbulent and non-evaporative conditions. It is used in SeaCluse as a relaxation term in the modelling of the macroscopic flux of the droplets due to ejection and gravitational fall (see (2.8) in chapter 2).

First, let us consider a single droplet, ejected at a position x at the wave surface. The probability ζ of finding the droplet in the height interval [z,z+Δz] is related to the time T(z,z+Δt) that the droplet spends in that height interval:

$$\zeta_{D,x}(z, z+\Delta z) = \frac{T(z, z+\Delta z)}{T_{fly}(D)} \qquad (4.9)$$

The x-dependency is removed by taking the sum of the contibutions of individual droplets ejected at various positions x over the wave surface:

$$\zeta_D(z, z+\Delta z) = \sum_{x=1}^{Nx} \zeta_{D,x}(z, z+\Delta z) \tag{4.10}$$

Which is renormalized by:

$$\zeta_D(z) = \lim_{\Delta z \to 0} \frac{\zeta_D(z, z+\Delta z)}{\int \zeta_D(z, z+\Delta z)\, dz} \tag{4.11}$$

The droplet concentration profile $\rho_D^0(z)$ in non-evaporative and non-turbulent conditions is found by multiplication with the density $\rho_{ej}(D)$ of droplets ejected at the wave surface:

$$\rho_D^0(z) = \rho_{ej}(D)\ \zeta_D(z) \tag{4.12}$$

The density $\rho_{ej}(D)$ will be discussed in chapter 6. At this stage, we restrict the calculation to the probabilities $\zeta_D(z)$.

The interval Δz in (4.9) is fixed to the maximum step-size $\delta p(D)$ in the trajectory calculation (see §4.2). This choice ensures that the droplet never moves more than one height interval Δz during one step Δt of the trajectory calculation. This facilitates the computation of $\zeta_D(z)$, but there is no specific reason why Δz cannot be smaller than the maximum value of $\delta p(D)$.

The number of individual profiles that are averaged to remove the x-dependency (see (4.10)) was first set to 20 (50 for D<100 μm). Figure 4.6a shows the resulting profile $\zeta_D(z)$ for D=200 μm. In this case, U_{10} = 10 m/s and the wave trough and crest are located at z = -0.73 m and z = +0.84 m, respectively. It is easily verified that 20 individual profiles are not sufficient to obtain a smooth average profile. In fact, the individual profiles can easily be recognized in figure 4.6a.

A rather large number of individual profiles is needed before the contributions of the individual profiles are no longer easily recognized in the average profile. Even then, the average profile is

not very smooth and a Gaussian smoothing routine[8] had to be applied. Figure 4.6b shows $\zeta_D(z)$ for D=200 μm and 100 individual profiles, and after smoothing.

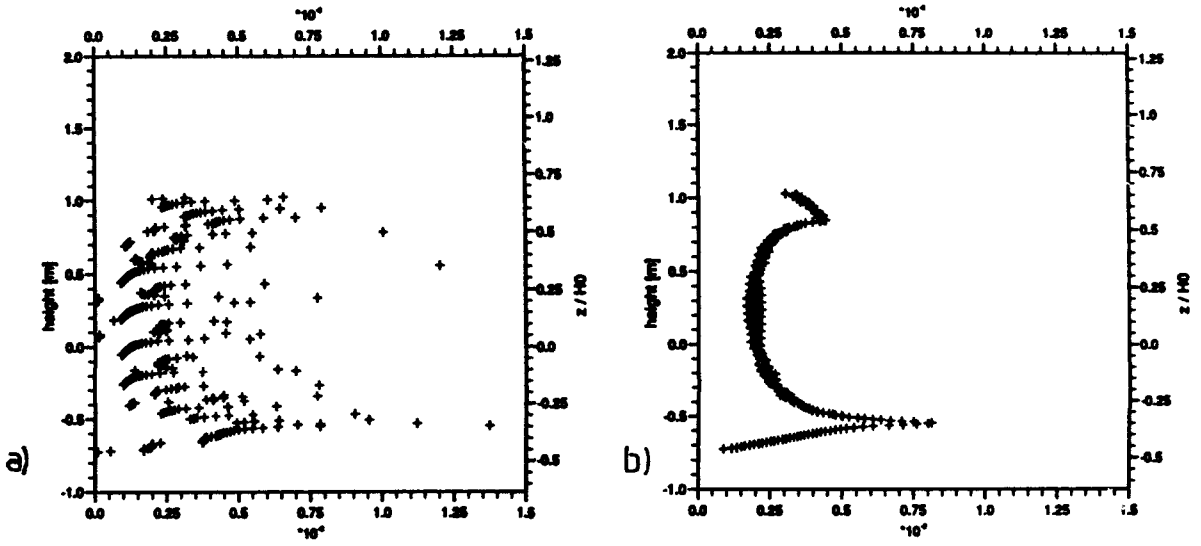

Figure 4.6: Normalized droplet profiles after averaging. Maxima are probably due to the choice of the wave profile
a) average of 20 individual profiles
b) average of 100 individual profiles and additional smoothing

The number Nx of individual profiles needed depends on the horizontal wind speed U_{10} (which determines the wave height) and varies between 50 (U_{10} < 5 m/s) and 200 (U_{10} > 16 m/s). In fact, Nx=200 is only just sufficient for the largest wind speeds for which the SeaCluse model is developed (U_{10} ≈ 25 m/s). However, with Nx=200 and U_{10} = 25 m/s, the CPU-time needed to calculate the profiles $\zeta_D^0(z)$ for droplets with D < 100 μm is very high (up to 30-40 min CPU-time for D=20 μm). An average over even more individual profiles would result in unacceptable computational demands.

8 In this routine, each datapoint x[i] is smoothed with the datapoints x[i-4]....x[i]....x[i+4]:
x[i] = α[1-4]x[i-4] + ... + α[i]x[i] + ... + α[i+4]x[i+4], where

$$\alpha[j] = e^{-\frac{|j-i|}{2\sigma}} / \sum_{k=i-4}^{k=i+4} \alpha[k] \quad \text{and} \quad \sigma = 1$$

5 MODEL FOR THE EVAPORATION OF SEA SPRAY DROPLETS

5.1 Parent and offspring categories

As pointed out by Mestayer [1990], salt water droplets must be described by at least two parameters: their radius r, and a parameter describing their chemical content. In the SeaCluse model this is done by defining parent categories, which contain the droplets with ejection radius $r_{ej}(i) \pm \Delta r_{ej}(i)$. Subsequently, offspring categories with radii $r_{off}(i,j) \pm \Delta r_{off}(i,j)$ are defined, which contain all droplets whose current radius is $r_{off}(i,j)$ and whose ejection radius was $r_{ej}(i)$. This leads to a model with variables that may have up to 3 indexes: parent category, offspring category and height. Thus, $V = V(i,j,z)$.

5.2 Andreas' model of evaporating sea spray droplets

Andreas [1989] started with eq.(13-26) of Pruppacher and Klett [1978] and showed that for sea spray droplets this equation could be rewritten as a set of three equations:

$$\dot{r} = \frac{\frac{\rho_v(z)}{\rho_{vs}(T(z))} - 1 - y}{\frac{\rho}{D_v' \rho_{vs}(T(z))} + \frac{L_v \rho}{T(z) k_a'} \left(\frac{L_v M_w}{R T(z)} - 1 \right)} \tag{5.1}$$

$$y = \frac{2 M_w \sigma_f}{R T(z) \rho_w r} - \frac{\gamma \phi m_s (M_w/M_s)}{m - m_s} \tag{5.2}$$

$$\rho = \rho_w \frac{1 + m/m_w}{1 + \nu_s \frac{\rho_w}{M_s} \frac{m}{m_w}} \tag{5.3}$$

where ρ denotes the density of the droplet; m, m_s and m_w the total mass of the droplet, the mass of water and the mass of salt in the droplet, respectively; ρ_w, ρ_v and ρ_{vs} the density of water, water vapor and saturated water vapor density, respectively; L_v the latent heat of evaporation; M_w and

M_s the molecular weight of water and NaCl, respectively; γ the number of ions into which NaCl dissociates; and [Pruppacher and Klett, 1978], [Millero, 1972]:

$$v_s(T) = v_{s0}(T) + S_v^*(T)\sqrt{c} \tag{5.4}$$

$$\phi(\mu/M_s) = -\frac{\ln a_w(\mu/M_s)}{v_s M_w \mu/M_s} \tag{5.5}$$

$$D_v'(T) = D_v(T)\left[\frac{r}{r+\Delta_w} + \frac{D_v(T)}{r\,\alpha_c}\sqrt{\frac{2\pi M_w}{R\,T}}\right]^{-1} \tag{5.6}$$

$$k_a'(T) = k_a(T)\left[\frac{r}{r+\Delta_r} + \frac{k_a(T)}{r\,\alpha_T\,\rho_a\,c_{pa}}\sqrt{\frac{2\pi M_a}{R\,T}}\right]^{-1} \tag{5.7}$$

In (5.4)-(5.7) v_s is the apparent molal volume, ϕ the practical osmotic constant, D_v' the modified molecular diffusivity of water vapor in air and k_a' the modified thermal conductivity of air. Other symbols are explained in appendix A and in the text below.

5.3 Mestayer's simplified model for sea spray droplet evaporation

Mestayer [1990] showed that Andreas' equations may be simplified with five assumptions, valid for $r > 1$ μm, $0 \le T \le 30$°C and RH ≥ 75% :

>1: The apparent molal volume v_s (eq.5.4) is not a function of temperature. In that case, the third equation of Andreas may be written as:

$$\rho(r) = \rho_w \frac{1+\mu(r)}{1+\frac{10^{-6}\,\mu(r)\,\rho_w}{M_s}\left(15+2.6\sqrt{\frac{10^{-3}\,\rho(r)\,S(r)}{M_s}}\right)} \tag{5.8}$$

where

$$\begin{cases} \mu(r) = \dfrac{m_s}{m_w} \\ S(r) = \dfrac{m_s}{m} = \dfrac{\rho_s}{\rho} \dfrac{r_{dry}^3}{r^3} = (\mu(r)^{-1} + 1)^{-1} \end{cases} \qquad (5.9)$$

S(r) is the salinity of the droplet. Equation (5.8) can be solved by an iterative procedure for a given value of r_{dry}.

>2: The practical osmotic coefficient ϕ (eq.5.5) is not a function of solution molality μ / M_s, but a constant.

>3: The first term in (5.2) may be neglected. This introduces only 1% error in the temperature and humidity range considered here. Assumptions 2 and 3 allow us to rewrite the second equation of Andreas as:

$$y(r) = - 0.6776\ \mu(r) \qquad (5.10)$$

where the values for the constants have been entered (with $\phi = 1.1$, the value at equilibrium at RH = 85%).

>4: The molecular diffusivity of water vapor in air D_v (eq.5.7) is not a function of temperature. In that case, (5.6) reduces to:

$$D_v'(r) = \frac{2.26\ 10^{-5}}{\dfrac{1}{1 + 8.10^{-8}\ r^{-1}} + 4.36\ 10^{-6}\ r^{-1}} \qquad (5.11)$$

where, once again, the values for the constants have been entered (with T = 283 K, and $D_v(283\ K) = 2.26\ 10^{-5}\ m^2/s$).

>5: The thermal conductivity of air k_a (eq.5.8) is not a function of temperature. In that case, (5.8) may be written as:

$$\frac{k_a'}{k_a} = f(r) \begin{cases} \geq 0.95 & r > 1\ \mu m \\ \approx 1.00 & r > 5\ \mu m \end{cases} \qquad (5.12)$$

For the range of radii considered here ($r > 1\ \mu m$), we may approximate:

$$k_a' = k_a = 0.0249 \qquad (T = 283\ K) \qquad (5.13)$$

Assumptions 4 and 5 allow us to rewrite the first equation of Andreas as:

$$r\dot{r} = \frac{\frac{\rho_v(z)}{\rho_{vs}(T(z))} - 1 - y(r)}{\frac{\rho(r)}{D_v'(r)\ \rho_{vs}(T(z))} + 1.004\ 10^8\ \frac{\rho(r)}{T(z)}\left(\frac{5417}{T(z)} - 1\right)} \qquad (5.14)$$

With these five assumptions equations (5.1)-(5.3) of Andreas are replaced by (5.14), (5.10) and (5.8), respectively. A closer inspection of the latter equations reveals that (5.8) and (5.10) contain only constants or variables depending on the droplet radius r and the dry radius r_{dry}. Thus, given the radii of the parent and offspring categories, the parameters y(r) and $\rho(r)$ are fixed.

5.4 The source terms in the SeaCluse model

Let us now turn to the modeling of the source-sink term $S_n(r)$ for droplets with radius r. Mestayer and Lefauconnier [1988] derived an expression for the source-sink term $S_n(r)$ for droplets (equation (2.9) in chapter 2):

$$S_n(r) = 6\ \rho_r \frac{\dot{r}}{r} - \dot{r}\frac{\partial \rho_r}{\partial r} - \rho_r \frac{\partial \dot{r}}{\partial r} \qquad (5.15)$$

under the conditions that the total number of droplets in the calculation domain is conserved and that the bins of the droplets are adjacent. In the above expression, ρ_r denotes the mass

concentration of droplets with radius r.[9] In contrast to Rouault et.al. [1991], who simplified (5.15) by assuming that the term r^2 (see (5.14)) depends only weakly on r, we will not further simplify (5.15).

Equation (5.15) governs the exchange between droplets of different radii. Since the evaporation of sea spray droplets with ejection radius $r_{ej}(i)$ is monitored via its offspring categories, droplets of different parent categories i_1 and i_2 are independent. Thus, we use (5.15) to calculate the exchange between a parent category $r_{ej}(i_1)$ and its various offspring categories $r_{off}(i_1,j)$, and we repeat this for all n parent categories:

$$\begin{cases} S_n(i) = \sum_{j=1}^{noff} S_n(i,j) \\ S_n = \sum_{i=1}^{n} S_n(i) \end{cases} \tag{5.16}$$

The total sum S_n allows us to calculate the source terms of temperature and water vapor, which couple all independent parent categories (see (2.3) and (2.5) in chapter 2):

$$\begin{cases} S_V = - S_n \\ S_T = \dfrac{L_v}{\rho_a c_{pa}} S_n \end{cases} \tag{5.17}$$

9 The use of the symbol ρ_r for droplet concentration (variable) may lead to confusion, because the symbol ρ is also used to denote densities of substances (constant). However, since droplet concentrations in the SeaClaus model are expressed in [kg/m^3], the symbol ρ_r seems appropriate.

6 IMPLEMENTATION IN THE SEACLUSE CODE

6.1 Calculation of radii of droplet categories

The radii of the offspring categories should be chosen in accordance with the expected shrinking of the droplets, which is limited to an equilibrium size determined by the ambient relative humidity. Therefore, Mestayer [1990] uses the lowest value of the relative humidity RH_{min} in the calculation domain to infer the smallest radius of the offspring categories by the procedure outlined below.

At equilibrium, $\dot{r} = 0$, and (5.14) reduces to:

$$y = \frac{\rho_v(z)}{\rho_{vs}(T(z))} - 1 = \frac{RH}{100} - 1 = -0.6776\,\mu \qquad (6.1)$$

where we have also used (5.10). In the case of equilibrium, y and μ no longer depend on the droplet radius r, but only on the relative humidity. Consequently, the salinity and droplet density are also independent of r (see (5.9)). The maximum mixing ratio in the domain is given by:

$$\mu_{max} = \frac{1}{0.6776}\left\{1 - \frac{RH_{min}}{100}\right\} \qquad (6.2)$$

Subsequently, (5.8) is solved iteratively to yield ρ_{max}, using (5.9b) to calculate the droplet salinity S_{max}, and with an initial value of $\rho = \rho_w$. Typically, this takes 5 iterations.

Equation (5.9) is used once more to infer a relation between the dry radius of the particle and its ejection radius. To this end, it is noted that the original salinity and density of the particle are equal to the salinity S_{sw} and density ρ_{sw} of sea surface water:

$$S_{sw} = \frac{\rho_s}{\rho_{sw}} \cdot \frac{r_{dry}^3}{r_{ej}^3} \quad \Rightarrow \quad r_{dry} = \frac{1}{3.96}\, r_{ej} \qquad (6.3)$$

Combining (6.3) and (5.9b), $r_{min}(i)$ of each parent category i can be calculated:

$$r_{min}(i) = r_{ej}(i) \left(\frac{1}{3.96} \sqrt[3]{\frac{\rho_s}{\rho_{max}} \frac{1}{S_{max}}} \right) = A_{max}\, r_{ej}(i) \qquad (6.4)$$

Finally, an equidistant radius grid is built for the n_{off} offspring categories (i,j) of parent category i:

$$\begin{cases} \Delta r(i) = \dfrac{r_{ej}(i) - r_{min}(i)}{n_{off} - 1} = r_{ej}(i) \dfrac{1 - A_{max}}{n_{off} - 1} \\ r(i,j) = r_{ej}(i) - (j-1)\, \Delta r(i) \qquad 1 \le j \le n_{off} \end{cases} \qquad (6.5)$$

Strictly speaking, there are only (n_{off}-1) offspring categories. For j=1 we have: $r(i,1) = r_{ej}(i)$, or in words, the parent category is also the first offspring category.

Relation (6.5a) furnishes the key of the grid of the parent categories, i.e., their bin widths are proportional to their nominal radius. This defines a non-equidistant parent grid: the smaller $r_{ej}(i)$, the smaller the bin width.

6.2 Calculation of r-dependent variables

As mentioned in the previous chapter, $D_v'(r)$ (eq.5.11), $\mu(r)$ (eq.5.8) and $\rho(r)$ (eq.5.9) may be calculated once the radii of the droplet categories have been determined. Unfortunately, (5.8) and (5.9) are coupled and have to be computed together in an iterative process. Mestayer [1990] gives the initial values for this calculation:

$$\begin{cases} \mu_0(r) = \dfrac{\rho_s}{\rho_w} \dfrac{1}{(r/r_{dry})^3 - 1} \\ \rho_0(r) = \rho_w \left[1 + \mu_0(r) \right] \end{cases} \qquad (6.6)$$

Typically, $\mu(r)$ and $\rho(r)$ converge after 10 iterations.

In principle, $\mu(r)$ and $\rho(r)$ are a function of both parent category i and offspring category j, that is:

$\mu(r) = \mu(i,j)$
$\rho(r) = \rho(i,j)$

However, we have chosen a radius grid in which n_{off} does not depend on i. In that case the ratio $r(i,j)/r_{ej}(i)$ is also independent of i. We may verify this by rearranging (6.5):

$$\frac{r(i,j)}{r_{ej}(i)} = 1 - \frac{(j-1)\,\Delta r(i)}{r_{ej}(i)} = 1 - \frac{(j-1)\,(1-A_{max})}{n_{off}-1} \qquad (6.7)$$

Consequently:

$\mu(r) = \mu(j)$
$\rho(r) = \rho(j)$

6.3 T_{fly} and V_f for droplet categories

Values for the flight time $T_{fly}(i,j)$ and final fall velocity $V_f(i,j)$ are retrieved from a database. In general, the database will not have entries for the radii r(i,j) and linear interpolation of the nearest entries r_+ and r_- is then used. When the radius r(i,j) is smaller than the smallest radius r_{min} in the database, the final fall velocity is approximated by the Stokes Velocity:

$$V_f(i,j) = -\frac{2}{9}\frac{\rho_w}{\rho_a}\frac{g}{\nu}\,r^2(i,j) \qquad (6.8)$$

This approximation is only correct for $r < 50$ μm [Rouault et.al., 1991], and SeaCluse issues a warning when $r > 50$ μm. When $r(i,j) < r_{min}$, the flight time is extrapolated from the first two entries r_1 and r_2 in the database:

$$\begin{cases} \dfrac{\delta T_{fly}}{\delta r} = \dfrac{T_{fly}(r_2) - T_{fly}(r_1)}{r_2 - r_1} \\ T_{fly}(i,j) = T_{fly}(r_1) - [r_1 - r(i,j)] \dfrac{\delta T_{fly}}{\delta r} \end{cases} \tag{6.9}$$

6.4 Initial and boundary conditions for SeaCluse

The initial conditions for the offspring categories should be identical to the initial conditions for the parent categories. In this manner, the model run starts with small (no) gradients $\partial\rho_r/\partial r$ (see (5.15)). Therefore, we use the initial condition previously given by Rouault et.al. [1991] (see also chapter 2):

$$\rho_r(i,j,z) = 0 \qquad \forall_{i,j,z} \tag{6.10}$$

We have not changed the boundary conditions at the top and the bottom of the calculation domain, that is, we use the equations given in chapter 2 for both the parent and the offspring droplets:

$$\rho_r(i,j,h_{tot}) = 0 \qquad \forall_{i,j} \tag{6.11}$$

$$\begin{cases} \rho_r(i,1,z_{min}) = \rho_{ej}(i) - \dfrac{\int_{z_{min}}^{z_{max}} S_n(i)\,dz + \rho_{ej}(i)\ V_{up}(i)}{V_f(i,1)} \\ \rho_r(i,j,z_{min}) = - \dfrac{\int_{z_{min}}^{z_{max}} S_n(i,j)\,dz}{V_f(i,j)} \qquad 2 \le j \le n_{off} \end{cases} \tag{6.12}$$

where $\rho_{ej}(i)$ denotes the concentration of ejected droplets with radius $r_{ej}(i)$ and we have used that $\rho_{ej} = 0$ for offspring categories. The boundary condition that the gradient in ρ_r must be zero at the top of the domain is not imposed, but is checked at the end of the model run (see below).

6.5 The model parameters C_1 and C_2 in SeaClue

Once again, we use expressions given previously by [Rouault et.al., 1991] to introduce the counterdiffusion and the macroscopic flux (see equations (2.7) and (2.8)), adapted for parent and offspring categories:

$$\begin{cases} \dfrac{1}{C_1 T_{fly}(i,1)} \left[\rho_r(i,1,z) - \rho_r^0(i,z) \right] & \\ \dfrac{1}{C_1 T_{fly}(i,j)} \left[\rho_r(i,j,z) \right] & 2 \le j \le n_{off} \end{cases} \tag{6.13}$$

$$Sc_t(i,j) = Sc_t \left[1 + C_2 \frac{V_f^2(i,j)}{1.56\, u_*^2} \right] \qquad 1 \le j \le n_{off} \tag{6.14}$$

where ρ_r^0 denotes the concentration profile of parent category i in non-turbulent, non-evaporative conditions (see chapter 4 and below). Obviously, $\rho_r^0 = 0$ for offspring categories since they only get populated by evaporation.

6.6 The droplet profiles in a non-turbulent, non-evaporative atmosphere

The vertical profiles of droplet concentration ρ_r^0 in non-turbulent and non-evaporative conditions are used in the modelling of the macroscopic flux of the droplets due to ejection and gravitational fall (see (2.8) in chapter 2). Normalized profiles $\zeta_0(i,z)$ have been calculated previously (see §4.5) and are available in a database. The numbers $\zeta_0(i,z)$ are converted into concentration $\rho_r^0(i,z)$ in [kg/m^3] by multiplication with the density $\rho_{ej}(i)$ of droplets ejected at the wave surface:

$$\rho_z^0(i,z) = \zeta(i,z)\ \rho_{ej}(i) \tag{6.15}$$

The density $\rho_{ej}(i)$ is found from the relation between the source function $\partial F/\partial r$ in $[m^{-2}s^{-1}\mu m^{-1}]$ and the flux of ejected droplets $\rho_{ej}(i)V_{up}(i)$:

$$\rho_{ej}(i) = \frac{\frac{\partial F(i)}{\partial r} \cdot \Delta r(i) \cdot \frac{4}{3}\pi\rho_w r_{ej}^3(i)}{V_{up}(i)} \tag{6.16}$$

where $\Delta r(i)$ is the size bin of parent category i. As a first guess, the source function $\partial F/\partial r$ is taken from Andreas [1992], who uses data from Miller [1987] for small droplets ($0.8\ \mu m \le r_{80} \le 15\ \mu m$):

$$\log\left(\frac{\partial F}{\partial r_{80}}\right) = B_0 + B_1(\log r_{80}) + B_2(\log r_{80})^2 + B_3(\log r_{80})^3 + B_4(\log r_{80})^4 \tag{6.17}$$

and data from Wu et.al. [1984] for larger droplets ($r_{80} > 15\ \mu m$):

$$\begin{cases} \frac{\partial F}{\partial r_{80}} = C_1\, r_{80}^{-1} & 15 \le r_{80} \le 37.5\ \mu m \\ \frac{\partial F}{\partial r_{80}} = C_2\, r_{80}^{-2.8} & 37.5 \le r_{80} \le 100\ \mu m \\ \frac{\partial F}{\partial r_{80}} = C_3\, r_{80}^{-8} & r_{80} \ge 100\ \mu m \end{cases} \tag{6.18}$$

In these source functions, r_{80} denotes the radius of the droplet at an ambient relative humidity of 80%. To convert r_{80} into r, Andreas [1989, 1992] gives the following conversion formula's:

$$\begin{cases} r_{80} = 0.518\, r^{0.976} \\ \dfrac{\partial F}{\partial r} = \dfrac{\partial r_{80}}{\partial r}\dfrac{\partial F}{\partial r_{80}} = 0.506\, r^{-0.024}\dfrac{\partial F}{\partial r_{80}} \end{cases} \tag{6.19}$$

The coefficients B_0-B_4 in (6.17) and C_1-C_3 in (6.18) are a function of U_{10}. Andreas [1992] tabulates values for these coefficients in the wind speed range 6-18 m/s. By interpolation, SeaCluse determines the value of $\partial F/\partial r$ for the value of U_{10} specified for the model run. Since extrapolation is not (yet) supported, the range of values of U_{10} in SeaCluse is restricted to 6-18 m/s.

The source function given above is by no means a consensus source function. The establishment of such a source function is rather difficult, because experimental data are sparse and hard to accomplish. An elaborate discussion of this subject would be outside the scope of this report (see Andreas [1992], and references therein). However, the validity of Andreas' source function is questionable [Katsaros and De Leeuw, 1993]. The two major objections are:

a) The dataset of Miller is small and shows a large amount of scatter in the region $10 \le r_{80} \le 15$ µm.
b) The dataset of Wu is based on data obtained in low-wind speed conditions ($U_{10} < 8$ m/s) and therefore not representative for spume droplets.

6.7 Calculation of the saturated water vapor density

In order to calculate the saturated water vapor density $\rho_{vs}(T)$ in (5.14), we use Buck's formula [1981] to compute the saturated water vapor pressure e_{sat}:

$$e_{sat}(T) = (1.0007 + 3.46\ 10^{6}\ P)\ 6.1121\ e^{\left(\frac{17.502\,\theta}{240.97+\theta}\right)} \tag{6.20}$$

where $\theta = T - 273.15$, and the standard pressure P=1013 mbar is used to obtain $e_{sat}(T)$ in mbar. Subsequently we apply the ideal gas law, as suggested by Andreas [1989] to compute the saturated water vapor density:

$$\rho_{vs}(T) = \frac{100\, M_w\, e_{sat}(T)}{R\, T} \qquad (6.21)$$

with T in K to obtain $\rho_{vs}(T)$ in [kg/m^3].

6.8 The vertical grid

The vertical grid in the SeaCluse model has to extend from the wave trough up to the top of the boundary layer. As mentioned previously, we have divided the vertical axis into two regions: a wave region below the wave crests and an atmospheric region above the wave crests. The origin of the vertical axis is located at mean sea level.

The grid in the wave region starts at a height z_0 above the wave trough (located at $z = -0.46\, H_0$). Our previous work on the CLUSE model for fresh water and the first tests of the SeaCluse model have shown that it is necessary to start with a small grid spacing. We found that the spacing should be of the order of the value of the eddy diffusivity, or the numerical solver will not work. Since the eddy diffusivity near the wave trough is rather small and the number of grid points is limited for computational reasons, a 'logarithmic' grid [Rouault et al., 1991] of 50 grid points is introduced:

$$\begin{cases} z[1] = -0.46\, H_0 + z_0 \\ z[i] = z[i-1] + \chi^{i-2}\, \Delta z[1] \qquad (2 \le i \le 50) \end{cases} \qquad (6.22)$$

where $\Delta z[1]$ is typically in the order 10^{-4} m and the irregularity parameter χ is chosen such that $\Delta z[50]$ is in the order of 1-5 centimeters.

The remainder of the wave region is covered by a linear grid, with a grid spacing equal to $\Delta z[50]$. In this manner we ensure that the region below the crests, where the production of sea spray aerosol takes place, is well covered by the grid. Continuing the non-linear grid would lead to an unacceptable large grid spacing near the crests. Thus:

$$z[i] = z[i-1] + \Delta z[50] \qquad (51 \le i \le N_{wave}) \qquad (6.23)$$

where N_{wave} is the total number of grid points in the wave region. To ensure that $z[N_{wave}]$ coincides exactly with the wave crest, the interval between $z[N_{wave}-1]$ and $z[N_{wave}]$ is somewhat enlarged or reduced.

The atmospheric region of the grid extends from the wave crests (at $z = 0.53H_0$) up to the top of the calculation domain (at $z = h_{tot}$). Since the exchange of vapor of the freshly generated sea spray aerosols mainly takes place in the lower regions of the atmosphere, it seems appropriate to use a grid in the atmospheric region which is more dense near the wave crests:

$$\begin{cases} z[i] = z[i-1] + \chi^{i-2}\,\Delta z[N_{wave}+1] \\ \Delta z[N_{wave}+1] = \dfrac{(h_{tot}-0.53H_0)(1-\chi)}{1-\chi^{N_{atm}}} \end{cases} \qquad (6.24)$$

where the number of grid points N_{atm} is adjusted to obtain an initial spacing $\Delta z[N_{wave}+1]$ that is *close to* $\Delta z[50]$. Typical values for the irregularity parameter χ are 1.04-1.08, leading to a grid spacing of 1-5 m at $z = 100$ m. The total number of grid points ($N_{wave} + N_{atm}$) is then in the order of 200.

6.9 Checks during the SeaCluse model run

During the model run, three checks with regard to the calculation of the source terms S_a, S_v and S_T are made:

>1: $f(i,j) > 0$ (see eq.5.14)

This means that $\partial r(i,j)/\partial t > 0$ and that the droplet tends to condensate. In other words, the SeaCluse model moves away from the correct solution. However, in the end the model should still be able to arrive at the correct solution, provided that the timestep of the model is sufficiently small. Therefore, the case $f > 0$ is noted, but no further action is taken.

>2: $\rho_r(i,j) < 0$ (see eq.5.15)

Although negative concentrations for any droplet category are physically impossible, we cannot just set $\rho_r(i,j)$ to 0. In that case we would violate the model constraint that the number of droplets is conserved. At the end of the model run, all $\rho_r(i,j)$ should be positive (again). Therefore, the case $\rho_r < 0$ is noted, but no further action is taken.

>3: $$\left(6\ \rho_r\ \frac{t}{r} \ -\ \rho_r\ \frac{\partial t}{\partial r} \right) > 0$$

The numerical method (see chapter 2) used in the model has the constraint that this part of (5.15) must be negative. Therefore, in the case that the above factor is positive, it is noted and the factor is reset to zero.

6.10 Checks at the end of the SeaCluse model run

At the end of the model run, three important checks related to the validity of the final results are made:

>1: The value RH_{min} of the relative humidity in the domain is determined. If RH_{min} is much lower than the value previously determined to set up the offspring radius grid (see §6.1), the radius grid may not extend to sufficiently small radii and droplets may not have been able to evaporate to their equilibrium sizes. In such a case, the calculation should be restarted with an extended offspring radius grid.

>2: The boundary condition $\partial\rho_v/\partial z = 0$ at the top of the calculation domain (see chapter 2) is not imposed during the model run. Therefore, it must be checked at the end of the model run to ensure that the number of droplets in the domain has been conserved.

>3: The convergence of the model solution is verified for the profiles of water vapor, temperature and droplets. Convergence is checked independently for water vapor, temperature and droplet concentration.

6.11 Presentation of final results

One of our aims is to compare the results of the SeaCluse model with experimental data obtained with (optical) particle counters or Rotorods. However, it is not possible to directly compare the model results and the data, because the experimental data is presented in adjacent size bins

$R_f(k)$ $\pm$½$\Delta R_f(k)$ and the model results in partly overlapping parent and offspring categories. In addition, the droplet concentrations in the SeaCluse model are expressed in [kg/m^3], whereas experimental data is often presented in [μm^2/cm^3].

Therefore, the parent and offspring categories r(i,j) $\pm$ ½Δr(i) must be mapped onto the radius grid $R_f(k)$ $\pm$ ½$\Delta R_f(k)$, once the model run is completed. The mapping is done by transferring a proportional part of $\rho_r(i,j)$ to $R_f(k)$ whenever the size bin of droplet category r(i,j) (partially) overlaps with a size bin $R_f(k)$. After this, we convert the ρ_r values (in kg/m^3) into dV/dr values (in μm^2/cm^3) by:

$$\frac{\partial V}{\partial r} = 10^{12} \frac{\rho_r}{\rho_w \Delta r} \qquad (6.25)$$

where Δr is in μm.

7 DISCUSSION AND AIMS OF FUTURE RESEARCH

The previous chapters have outlined the SeaCluse model, which extends the CLUSE model to 'open ocean' conditions. Several new hypotheses had to be made in order to describe the air flow over the waves (chapter 3):

1. The waves are modelled by a 2-dimensional Stokes wave
2. The waves are fully developed
3. Momentum is only transferred to the water (no form drag)
4. The atmospheric stratification is neutral

An additional hypothesis was introduced to describe the movement of the droplets in the air flow (chapter 4):

5. The droplet flight times in non-turbulent and non-evaporative conditions are finite

Furthermore, approximations were made in the equations that govern the evaporation of salt water droplets (chapter 5). These limit the applicability of the SeaCluse model to:

$r > 1\ \mu m$ $\quad 0 \leq T \leq 30\ ^{\circ}C$ $\quad RH \leq 75\%$

Whether or not the new hypotheses are acceptable cannot be discussed here, because the SeaCluse model has not yet been tested and validated with experimental data from the HEXOS program [De Leeuw, 1990a]. Testing, and subsequent comparison of the model results with experimental data will be the primary objective in the continuation of this research.

The outcome of these tests determines whether our model for the air flow over the waves needs to be further elaborated. Also, it may be necessary to modify or to replace the aerosol droplet source function (see the discussion in chapter 1 and 6.6). New and more detailed experimental results on the number of jet droplets released from bursting bubbles, their ejection heights and their velocities will be available soon [Spiel, 1992a and 1992b] and may be included in the SeaCluse model.

The SeaCluse model only takes jet droplets into account, neglecting film droplets that are also produced from bursting bubbles. In fact, the larger bubbles produce no jet drops at all, only film droplets [Blanchard, 1983]. Even so, the relative contribution of film drops is small [Wu, 1989], because the film droplets are very small and are ejected with small vertical velocities. Therefore, we feel that neglecting the film droplets is justified.

In addition to the bubble-mediated production, spume droplets may be directly produced by wave tearing. This mechanism comes into play at wind speeds exceeding 9 m/s [Monahan et.al., 1986]. The question as to what extent the spume droplets contribute to the total droplet flux has not yet been definitively answered. Wu [1990] estimates a contribution of 33% at wind speeds of 13 m/s, based on experimental data by De Leeuw [1986]. On the other hand, more recent experimental evidence by De Leeuw [1990b] shows that spume droplets are unlikely to contribute much to the total aerosol concentrations at this wind speed.

The SeaCluse model may be extended with a module that describes the production of spume droplets at the wave crests. In this manner, the effect of spume drops on the humidity profile and the heat fluxes can be studied. However, it should be emphasized that only qualitative results are to be expected in the absence of a reliable aerosol source function.

Our model of the air flow over the waves leads essentially to a wave-rotor between the wave crests (compare figures 1.2 and 3.7). The wave rotor model has been proposed by De Leeuw [1986] to explain the observed minima and maxima in the particle concentration profiles ($10 < D < 100$ μm) between 0.2 and 20 m AMSL [De Leeuw, 1986, 1987]. With our wave-rotor model, we conjecture that the largest droplet concentrations will exist in the lee side of the waves. This conclusion is based on the extended droplet suspension times at that location and the droplet trajectories (see figures 4.1 and 4.2).

This is in accordance with laboratory experiments by Koga and Toba [1981], who also observed larger concentrations at the lee side of the waves, resulting from droplets produced at the downward slope of the same wave trough. On the other hand, De Leeuw [1989c] indicated that in the field the production may be higher on the windward side of the crest, because the whitecap of a trailing wave can be at the windward side of the crest. This could be an impetus to include a module in SeaCluse that describes the wave breaking.

The SeaCluse model yields information on the vertical structure of the atmosphere (water vapor, droplet distribution, temperature), from which important parameters such as the refractive index and the extinction may be inferred. Therefore, the model could be used to assess the maximum effective range of electro-optical sensors. One of the requirements for an operational range predictor is that the input parameters can be easily obtained. In this respect, the SeaCluse model is nearly perfect: its input consists of only four parameters, that can be obtained by standard instrumentation: U_{10} RH_{10} T_{10} T_{surf}.

In addition, the SeaCluse model uses the droplet source function given by Andreas [1992]. This function (see §6.6) is a function of U_{10} only.

Theoretically, the smallest droplets that can be handled by the SeaCluse model have a radius of 1 μm. However, computational demands become rather high when the droplet radius is in the order of a few microns. This is a severe drawback for the application of the model in range prediction, since droplets with radii smaller than 10 μm determine the visibility in the visible wavelength region and contribute appreciably to the visibility in the IR.

In order to overcome this drawback, the CLUSA model is being developed at the Ecole Centrale de Nantes [Mestayer et.al., 1991]. CLUSA describes the dispersion of a distribution of aerosols from 0.05 to 2.5 μm radius in the marine atmospheric surface layer. In its present state, CLUSA starts from an initial profile of dry aerosol that is transformed to marine conditions by calculating the aerosol growth by water vapor condensation. Subsequently, the effective deposition velocity of the aerosols is calculated as a function of their original size and chemical composition, of the hygro-thermodynamic atmospheric condition, and of the sea state. The calculation includes gravitational settling, Brownian diffusion and the presence of the diffusive sub-layer close to the sea surface.

In the future, merging CLUSA and SeaCluse, the model should include the interactions of the smaller aerosols with sea spray droplets by coalescence and with the water vapor field. The combined model would then govern the complete size range of aerosols that determine the propagation properties of the atmosphere.

The SeaCluse model only deals with freshly produced sea-spray aerosols. The total aerosol concentration in the atmosphere results from a balance between local production and removal and

the advection of aerosol produced elsewhere. It is conjectured that the advected aerosol is in effect a 'background' that adds to the profile due to the locally produced aerosol. In view of the long mixing times, the latter constitutes only a small fraction of the total aerosol concentration.

The background aerosol consists of a mixture of man-made, biological and natural aerosol of continental and marine origin, containing a large variety of hygroscopic and non-hygroscopic species which strongly influence the dependence on relative humidity. Furthermore, aerosol droplets are not inert and their composition can change through many chemical reactions which take place in the atmosphere.

Van Eijk and De Leeuw [1992] recently addressed the importance of taking the background aerosol of continental origin into account when predicting propagation parameters (e.g., atmospheric extinction) for a coastal region. Apparently, well-established aerosol models such as the Navy Aerosol Model [Gathman, 1983] fail for 'polluted inner seas' like the North Sea and the Mediterranean [Tanguy et.al., 1991].

In conclusion, a model that aims to provide an adequate description of the propagation properties of the atmosphere cannot be confined to the freshly produced sea-salt aerosols. In addition, modules that handle the continuously changing chemical composition and the dispersion of the 'background' aerosols are needed. Only then the model can truly govern the production, advection and deposition of the aerosols.

8 ACKNOWLEDGEMENT

This work has been sponsored in part by the Netherlands Ministry of Defense under contract A90KM638 and by the Commission of the European Communities (EC DG XII contract STEP-CT-0047), and, as an Eurotrac ASE Contribution by the French Centre National de la Recherche Scientifique (92N82/0019 Environnement). Part of the work described in this report was performed while A.M.J. van Eijk held the position of "enseignant invité" at the Ecole Centrale de Nantes.

9 REFERENCES

Andreas, E.L. [1989]. Thermal and size evolution of sea spray droplets. Cold Regions Research & Engineering Laboratory report, Hanover, NH, USA, CRREL-Report 89-11.

Andreas, E.L. [1992]. Sea spray and turbulent air-sea fluxes. J. Geophys. Res C97, 11429-11441.

Beard, K.V. and Pruppacher, H.R. [1971]. A wind tunnel investigation of the rate of evaporation of small water drops falling at terminal velocity in air. J. Atmos. Sci. 28, 1455-1464.

Blanchard, D.C. [1963]. The electrification of the atmosphere by particles from bubbles in the sea. Prog. Oceanogr. 1, 71-202.

Blanchard, D.C. and Woodcock, A.H. [1980]. The production, concentration and vertical distribution of the sea-salt aerosol. Ann. of the NY Academy of Science, 330-347.

Blanchard, D.C. [1983]. The production, distribution, and bacterial enrichment of the sea-salt aerosol. In: Air-Sea exchange of gases and particles, 407-454, P.S. Liss and W.G.N. Slinn (eds.), Reidel, Dordrecht, NL.

Blanchard, D.C. [1989]. The size and height to which jet drops are ejected from bursting bubbles in seawater. J. Geophys. Res. 94, 10999-11002.

Buck, A.L. [1981]. New equations for computing vapor pressure and enhancement factor. J. Applied Meteorol. 20, 1527-1532.

Charnock, H. [1955]. Wind stress on a water surface. Quart. J. Royal Met. Soc. 81, 639-640.

Davidson, K.L., DeCosmo, J., De Leeuw, G., Edson, J.B, Katsaros, K.B., Mengelkamp, H.T., Oost, W.A., Smith, S.D. and Taylor, P.K. [1993]. Variation of wind, stress, heat and vapor fluxes in vicinity of fronts. In preparation.

Dekker, H. and DeLeeuw, G. [1993]. Bubble excitation of surface waves and aerosol droplet production: a simple dynamical model. Accepted for publication in J. Geophys. Res.

DeLeeuw, G. [1986]. Vertical profiles of giant particles close above the sea surface. Tellus 38B, 51-61.

DeLeeuw, G. [1987]. Near-surface particle size distributions profiles over the North Sea. J. Geophys. Res. 92, 14631-14635.

DeLeeuw, G., Davidson, K.L., Gathman, S.G. and Noonkester, R.V. [1989a]. Physical models for aerosols in the marine mixed layer. AGARD-CP 453, 40-1 to 40-8.

DeLeeuw, G. [1989b]. The occurrence of large salt water droplets at low elevations over the open ocean. In: The climate and health implications of bubble mediated sea-air exchange, 65-82, E.C. Monahan and M.A. Van Patten (eds). Connecticut Sea Grant college Program CT-SG-89-06.

DeLeeuw, G. [1989c]. Investigations on turbulent fluctuations of particle concentrations and relative humidity in the marine atmospheric surface layer. J. Geophys. Res. C94, 3261-3269.

DeLeeuw, G. [1990a]. Profiling of aerosol concentrations, particle size distributions and relative humidity in the atmospheric surface layer over the North Sea. Tellus 42B, 342-354.

DeLeeuw, G. [1990b]. Comment on "Vertical distributions of spray droplets near the sea surface: influences of jet drop ejection and surface tearing", by J. Wu. J. Geophys. Res. C95, 9779-9782.

DeLeeuw, G., Larsen, S.E., Mestayer, P.G., van Eijk, A.M.J., Dekker, H., Zoubiri, A., Hummelshøj, P. and Jensen, N.O. [1991]. Aerosols in the marine atmospheric surface layer: production, transport and deposition. EUROTRAC annual report 1991 part 3, 61-67.

DeLeeuw, G. [1993]. Aerosols near the air-sea interface. To be published in 'Trends in Geophysical Research'.

Edson, J.B. [1989]. Lagrangian model simulation of the turbulent transport of evaporating jet droplets. Ph.D. Thesis, Dept. Meteorology, Penn. State University, USA.

Edson, J.B. [1990]. Simulating droplet motion above a moving surface. In: Modelling the fate and influence of marine spray, 84-94, P.G. Mestayer, E.C. Monahan and P.A. Beetham (eds), Marine Sciences Institute, University of Connecticut.

Edson, J.B., Fairall, C.W., Mestayer, P.G. and Larsen, S.E. [1991]. A study of the inertial-dissipation method for computing air-sea fluxes. J. Geophys. Res. 96C, 10689-10711.

Fairall, C.W., Davidson, K.L. and Schacher, G.E. [1983]. An analysis of the surface production of sea-salt aerosols. Tellus 35B, 31-39.

Garatt, J.R. [1977]. Review of drag coefficients over oceans and continents. Mon. Weather Review 105, 915-929.

Gathman, S.G. [1983]. Optical properties of the marine aerosol as predicted by the Navy Aerosol Model. Opt. Eng. 22, 57-62.

Gathman, S.G. [1989], A preliminary description of NOVAM, the Navy Oceanic Vertical Aerosol Model. NRL Report 9200 (Washington, D.C.).

Geernaert, G.L., Katsaros, K.B. and Richter, K. [1986]. Variation of the drag coefficient on sea state. J. Geophys. Res. 91, 7667-7679.

Geernaert, G.L. [1988]. Drag coefficient modeling for the near coastal zone. Dyn. of. Atmos. and Oceans, 11, 307-322.

Geernaert, G.L. [1990]. Bulk parameterizations for the wind stress and heat fluxes. In: Surface waves and fluxes, Volume I, 91-172, G.L. Geernaert and W.J. Plant (eds), Kluwer Academic Press, Dordrecht, NL.

Gerber, H.E. [1985]. Relative humidity parameterization of the Navy Aerosol Model (NAM). NRL Report 8956 (Washington, D.C.).

Hughes, H.G. [1987]. Evaluation of the LOWTRAN 6 Navy maritime aerosol model using 8 to 12 μm sky radiances. Opt. Eng. 26, 1155-1160.

Katsaros, K.B. and DeLeeuw, G. [1993]. To be published.

Kitaigorodski, S.A., Kuznetsov, O.A. and Panin, G.N. [1973]. Coefficients of drag, sensible heat, and evaporation in the atmosphere over the surface of the sea. Izv. Atmos. Ocean. Phys. 9, 1135-1141.

Kneizys, F.X., Shettle, E.P., Gallery, W.O., Chetwynd Jr., J.H., Abreu, J.H., Selby, J.E.A. Clough, S.A. and Fenn, R.W. [1983]. Atmospheric transmittance/radiance: computer code LOWTRAN 6. Air Force Geophysics Laboratory, report AFGL-TR-83-0187, Hansom Air Force Base, Bedford MA, U.S.A.

Koga, M. and Toba, Y. [1981]. Droplet distributions and dispersion processes on breaking wind waves. Sci. Rep. Tohoku Univ., Ser.5 (Tohoku Geophys. J.) 28, 1-25.

Kuypers, L. and Tinman, R. (eds) [1963]. Handbook of mathematics. Pergamon Press, Oxford.

Larsen, S.E., Edson, J.B., Mestayer, P.G., Fairall, C.W. and DeLeeuw, G. [1990]. Sea spray and particle deposition, air/water tunnel experiment and its relation to over-ocean conditions. In: Proc. of EUROTRAC Symposium '90, 71-75. P. Borrell et al. (eds). Academic Publ., The Hague, NL.

Ling, S.C. and Kao, T.W. [1976]. Parameterization of the moisture and heat transfer process over the ocean under whitecap sea states. J. Phys. Oceanogr. 6, 306-315.

Maat, N., Kraan, C. and Oost, W.A. [1991]. The roughness of wind waves. Bound. Layer. Meteorology 54, 89-103.

MacIntyre, F. [1968].A boundary layer 'microtome' for micron-thick samples of a liquid surface. J. Phys. Chem. 72, 589.

MacIntyre, F. [1972]. Flow patterns in breaking bubbles. J. Geophys. Res. 77, 5211-5228.

Melville, W.K. and Bra, K.N.C. [1979]. A model of the two-phase turbulent jet. Int. J. Heat Mass Transfer 22, 647-656.

Mestayer, P.G. and Lefauconnier, C. [1988]. Spray droplet generation, transport and evaporation in tunnel during the Humidity Exchange Over the Sea Experiments in simulation tunnel. J. Geophys. Res. 93, 572-586.

Mestayer, P.G. et al. [1988]. HEXIST. W.A. Oost, S.D. Smith and K.B. Katsaros (eds.). Proceeding NATO Advanced Workshop on Humidity Exchange Over the Sea Main Experiment (HEXMAX) technical report, 154-163. Dept.Atmos.Sci, Univ.of Washington, Seattle, U.S.A.

Mestayer, P.G. [1990]. Sea water droplet evaporation in the CLUSE model. In: Modelling the fate and influence of marine spray, 65-76, P.G. Mestayer, E.C. Monahan and P.A. Beetham (eds), Marine Sciences Institute, University of Connecticut.

Mestayer, P.G., Zoubiri, A. and Edson, J.B. [1991]. Experimental and numerical study of aerosol dynamics and deposition at the sea surface; 2PIE, GWAIHIR & CLUSA. EUROTRAC Annual Report 1990, 66-74.

Miller, M.A. [1987]. An investigation of aerosol generation in the marine planetary boundary layer. M.S. Thesis, Dept. Meteorology, Penn. State University, USA.

Miller, M.A. and Fairall, C.W. [1988]. A new parameterization of spray droplet production by oceanic whitecaps. In: Proceedings of the 7th conference on ocean-atmosphere interaction, American Meteorological Society, Boston MA, U.S.A.

Millero, F.J. [1972]. The partial molal volumes of electrolytes in aqueous solution. In: R.A. Horne (ed), Water and aqueous solutions, 519-595, Wiley, New York.

Monahan, E.C., Davidson, K.L. and Spiel, D.E. [1982]. Whitecap aerosol productivity deduced from simulation tank measurements. J. Geophys. Res. 87, 8898-8904.

Monahan, E.C., Spiel, D.E. and Davidson, K.L. [1986]. A model of marine aerosol generation via whitecaps and wave disruption, 167-174. In: E.C. Monahan and G. McNiocaill (eds.), Oceanic Whitecaps, Reidel, Dordrecht, NL.

Patankar, S.V. and Spalding, D.B. [1970] Heat and Mass transfer in boundary layers: a general calculation procedure. Intertext book, London, 2nd ed.

Pruppacher, H.R. and Klett, J.D. [1978]. Microphysics of clouds and precipitation. Reidel, Dordrecht, NL.

Raudviki, A.J. [1979]. Loose boundary hydraulics. Pergamon, New York.

Rouault, M.P. [1989]. Modélisation numérique d'une couche limite unidimensionelle stationnaire d'embruns. Thèse de Doctorat, Université d'Aix-Marseille II, France.

Rouault, M.P. and Larsen, S.E. [1990]. Spray droplets under turbulent conditions. Risø National Laboratory, report Risø-M-2847, February 1990.

Rouault, M.P., Mestayer, P.G. and Schiestel, R. [1991]. A model of evaporating spray droplet dispersion. J. Geophys. Res. 96, 7181-7200.

Schiestel, R. [1991]. Unpublished results.

Smith, S.D. [1980]. Wind stress and heat flux over the ocean in gale force winds. J. Phys. Ocean 10, 709-726.

Smith, S.D. [1988]. Coefficients for sea surface wind stress, heat flux, and wind profiles as a function of wind speed and temperature. J. Geophys. Res. 93, 15467-15472.

Smith, S.D., Katsaros, K.B., Oost, W.A. and Mestayer, P.G. [1990]. Two major experiments in the Humidity Exchange Over the Sea (HEXOS) program. Bull. Am. Meteor. Soc. 71, 161-172.

Spiel, D.E. [1992a]. Acoustical measurements of air bubbles bursting at a water surface: bursting bubbles as Helmholtz resonators. J. Geophys. Res C97, 11443-11452.

Spiel, D.E. [1992b]. Personal communication.

Tanguy, M., Bonhommet, H., Autric, M. and Vigliano, P. [1991]. Correlation between the aerosol profiles measurements, the meteorological conditions and the IR transmission in a Mediterranean marine atmosphere. SPIE Proceedings 1487, 17-1 to 17-12.

Van Eijk, A.M.J and DeLeeuw, G. [1992]. Modeling aerosol extinction in a coastal environment. SPIE Proceedings 1688, 28-36.

White, F.M. [1988]. Fluid Mechanics. McGraw Hill, New York.

Wu, J. [1974]. Evaporation due to spray. J. Geophys. Res. 79, 4107-4109.

Wu, J. [1979]. Spray in the atmospheric surface layer: Review and analysis of laboratory and oceanic results. J. Geophys. Res. 84, 2959-2969.

Wu, J. [1980]. Wind stress coefficients over the sea surface near neutral conditions - a revisit. J. Phys. Oceanogr. 10, 727-740.

Wu, J., Murray, J.J. and Lai, R.J. [1984]. Production and distributions of sea spray. J. Geophys. Res 89, 8163-8169.

Wu, J. [1989]. Contributions of film and jet drops to marine aerosols produced at the sea surface. Tellus 41B, 469-473.

Wu, J. [1990]. Vertical distributions of spray droplets near the sea surface: influences of jet drop ejection and surface tearing. J. Geophys. Res. C95, 9775-9778.

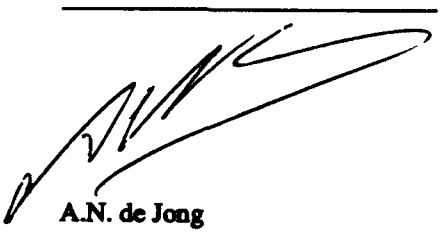

A.N. de Jong
(Group leader)

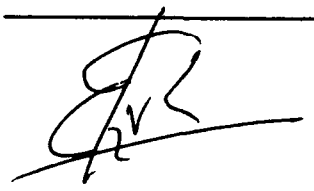

A.M.J. van Eijk
(Project leader/author)

NOMENCLATURE

Symbol	Unit	
a_w		water activity of an aqueous solution
c	mol/l	molar concentration of an aqueous solution
c_{ps}	J/kgK	specific heat of air at constant pressure
C_{DN}		Drag coefficient (neutral stratification)
C_s	m/s	phase velocity of the waves
D	m	diameter
D_v	m^2/s	molecular diffusivity of water vapor in air
D_v'	m^2/s	modified D_v
g	m/s^2	acceleration of gravity
h_{tot}	m	height of the calculation domain
H_{ej}	m	jet droplet ejection height
H_0	m	wave amplitude
i		index of parent categories
j		index of offspring categories
k	m^{-1}	propagation constant
k_a'	W/mK	modified thermal conductivity of air
L_v	J/kg	latent heat of vaporization of water
m	kg	mass of the droplet
m_s	kg	mass of NaCl in the droplet
m_w	kg	mass of pure water in the droplet
M_a	kg	molecular weight of air
M_s	kg	molecular weight of NaCl
M_w	kg	molecular weight of water
n		number of parent categories
noff		number of offspring categories
Nx		number of horizontal grid points
Nz		number of vertical grid points
Pr_t		Prandtl number
r	m	radius of droplet
r_{dry}	m	dry radius of the droplet
r_{ej}	m	radius of parent category (ejection radius)
r_{off}	m	radius of offspring category
R	J/mol,K	universal gas constant
Re		Reynolds number
RH	%	relative humidity

RH_{surf}	%	relative humidity at the surface
RH_{10}	%	relative humidity at z = 10 m
S		salinity of the droplet
S_n		source-sink term for droplets
S_{sw}		salinity of sea surface water
S_T		source term of temperature
S_V		source term of water vapor
S_v^*	$m^3l/$ $mol^{3/2}$	function of T in finding the apparent molar volume of an aqueous solution
Sc_t		Schmidt number
T	K	temperature
T_{fly}	s	flight or suspension time of droplet
T_{surf}	°C	sea surface temperature
T_{10}	°C	temperature at z = 10 m
T_*	°C	temperature scaling factor
U	m/s	horizontal wind speed
U_{10}	m/s	horizontal wind speed at z = 10 m
u_d	m/s	horizontal speed of droplet
u_r	m/s	horizontal speed of droplet, relative to air
u_*	m/s	friction velocity
v_a	m^2/mol	apparent molal volume of an aqueous solution
v_{a0}	m^2/mol	v_a at infinite dilution
V_f	m/s	final fall velocity of the droplet
V_{up}	m/s	droplet ejection velocity
W	m/s	vertical wind speed
w_d	m/s	vertical speed of droplet
w_r	m/s	vertical speed of droplet, relative to air
t	s	time
x		horizontal coordinate
z	m	vertical coordinate, z = 0 at mean sea level
z_0	m	roughness length calculated with Charnock or Kitaigorodski model
z_{0L}	m	z_0 for local profiles of U, ρ_v and T
z_{0a}	m	z_0 for the atmospheric profile U(z)
α_c		empirical constant used in computing D_v'
α_T		empirical constant used in computing k_a'
γ		total number of ions into which a salt molecule in the droplet dissociates
δp	m	step size in droplet trajectory calculation
Δ_T	m	empirical length scale used in computing k_a'
Δ_w	m	empirical length scale used in computing D_v'

Appendix A
NOMENCLATURE

Δr	m	size bin of droplet category
Δt	s	time step in droplet trajectory calculation
η	m	height of the wave surface
κ		Von Karman constant
λ	m	length of the wave
μ		mass mixing ratio of NaCl and H_2O in the droplet
ν	m^2/s	kinematic viscosity of air
ρ	kg/m^3	density of droplet
ρ_a	kg/m^3	density of dry air
$\rho_D{}^0$	kg/m^3	concentration of droplets of diameter D in non-evaporative and non-turbulent conditions
ρ_{ej}	kg/m^3	concentration of droplets ejected from the surface
ρ_r	kg/m^3	concentration of droplets with radius r
ρ_s	kg/m^3	density of NaCl
ρ_{sw}	kg/m^3	density of sea surface water
ρ_v	kg/m^3	water vapor density
ρ_{vs}	kg/m^3	saturated water vapor density
ρ_{v^*}	kg/m^3	scaling factor for humidity profile
ρ_w	kg/m^3	density of water
σ_f	J/m^2	surface tension of a flat surface with the same salinity and temperature as the droplet
σ_t	m^2/s	eddy diffusivity
ϕ		practical osmotic coefficient of the droplet
ϕ_m		atmospheric stability function
χ		irregularity of vertical grid
ω	s^{-1}	wave period

THE WAVE GRID

When a variable is to be averaged over the wave surface, a grid is needed that is equidistantly spaced over the wave surface. This is not the same as a grid equidistantly spaced in z or x, because the wave surface has to be followed. When we denote the coordinate along the wave surface by s, the trajectory along the wave surface may be calculated by a triangular method:

$$\frac{\Delta z}{\Delta x} = \tan \alpha \quad ; \quad \cos \alpha = \frac{\Delta x}{\Delta s} \tag{B.1}$$

Thus, for sufficiently small triangles (say, 1000 over a wave period), we may calculate Δs with (B.1), using the derivative of the Stokes wave (see equation 3.3):

$$\frac{\partial z}{\partial x} = \frac{\pi}{20} \sin (kx-\omega t) - \frac{\pi^2}{400} \sin (2(kx-\omega t)) \tag{B.2}$$

The total path length S along the wave surface is equal to:

$S = \Sigma \Delta s$

If we neglect the curvature of the wave by taking an x-grid, the path length X is given by:

$X = \Sigma \Delta x$

We calculated both X and S and it turned out that S is only 0.6% longer than the horizontal path length X. Therefore, we make only a minor error if we replace the wave surface grid (along s) by a horizontal grid (along x). The physical reason for this is that the length of the Stokes wave is 20 times its amplitude, i.e., the slope of the wave surface is rather low.

EDDY DIFFUSIVITY IN THE WAVE ROTOR APPROXIMATION

When we assume that the wave rotor plays an dominant role below the wave crests, the eddy diffusivity in that region is given by:

$$\begin{cases} \sigma_t(z,t) = \sigma_t(\text{crest}) & z > \eta(t) \\ \sigma_t(z,t) = 0 & z < \eta(t) \end{cases} \tag{C.1}$$

where $\eta(t)$ is the instantaneous wave height at time t. To calculate σ_t below the wave crests, we need to know $t_+(z)$, i.e., the amount of time that height z is above the wave surface (relative to the wave period T_0).

We may obtain $t_+(z)$ from the expression for the Stokes wave (eq.3.3). To this end, we set x = 0, which yields:

$$\eta(t) = -\frac{H_0}{2}\cos(-\omega t) + \frac{\pi H_0}{80}\cos(-2\omega t) \tag{C.2}$$

Subsequently, this equation is inverted for $0 \le t \le \frac{1}{2}T_0$. Using the goniometric rule $\cos 2\beta = 2\cos^2\beta - 1$ and the abc-rule for quadratic expressions, this yields:

$$t_+(z) = \frac{1}{\pi}\arccos\left\{ \frac{\frac{1}{2}H_0 \pm \sqrt{\frac{1}{4}H_0^2 + \frac{\pi}{10}H_0 z + \frac{\pi^2}{800}H_0^2}}{\frac{\pi}{20}H_0} \right\} \tag{C.3}$$

The eddy diffusivity below the wave crests is then given by:

$$\sigma_t(z) = t_+(z)\,\kappa\,\sigma_t(\text{crest}) \qquad z < \frac{1}{2}H_0 \tag{C.4}$$

An example of this calculation is shown in figure C.1. Below the wave crests, the eddy diffusivity follows the inverse of the Stokes wave, whereas above the waves the linear relation (eq.3.10)

applies. There is a small discontinuity at the wave crest caused by rounding errors. I.e., at the wave crest σ_t as calculated by the linear function is not exactly equal to σ_t as calculated by the inverse function. Typically, the difference amounts to 0.5%.

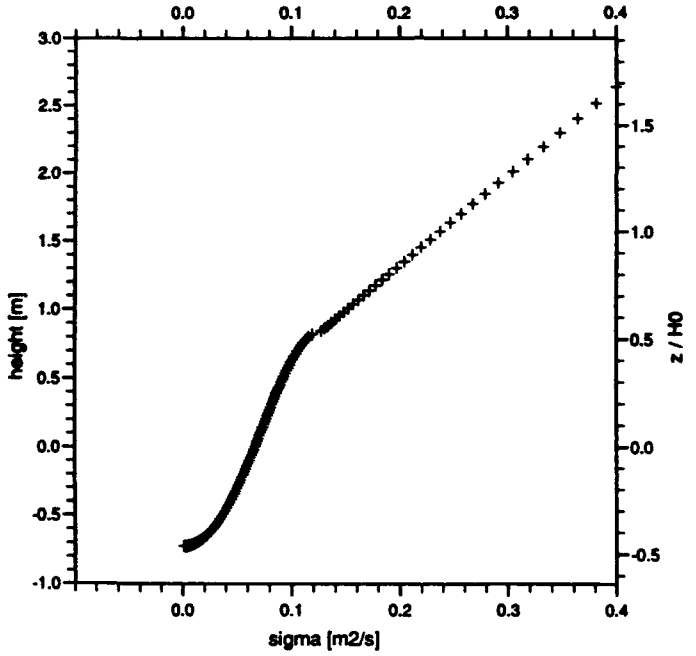

Figure C.1: Eddy diffusivity calculated with the wave rotor approximation

CHARNOCK RELATION AND KITAIGORODSKI MODEL

The SeaCluse model calculates the roughness length z_0 by Charnock's relation or the Kitaigorodksi model for verification purposes (see §3.4).

Charnock's relation [Charnock, 1955] is given by:

$$z_0 = a_c \frac{u_*^2}{g} \tag{D.1}$$

where $a_c = 0.011$ for open ocean [Smith, 1988] and $a_c = 0.019$ for coastal areas (average value from [Garatt, 1977], [Wu, 1980] and [Geerneart et al., 1986]).

For open ocean conditions, we may also calculate the roughness length z_0 by the Kitaigorodski model [Kitaigorodski et al., 1973], given by:

$$z_0 = A_K \left[\int_0^\infty S(\omega)\ \exp(-2\kappa g/\omega u_*)\ d\omega \right]^{0.5} \tag{D.2}$$

where $A_K = 0.028$ [Geernaert, 1988] and $S(\omega)$ denotes the wave spectrum. In our model, $S(\omega)$ is taken to be a Philips wave spectrum:

$$S(\omega) = \beta\, g^2\, \omega^{-5} \qquad \omega > \omega_0 \tag{D.3}$$

where ω_0 denotes the frequency of the Stokes wave (see equation 3.3) and β is given by Geerneart et al., [1986]:

$$\beta = 0.005 + 0.002\omega + 1.5(g/\omega_0 u_*)^{-2} \tag{D.4}$$

for open ocean conditions. Note that this relation for β was established for wave spectra measured during the MARIEN experiment for unlimited fetch conditions but for water depths of only 15 meter. For application to coastal seas, this model should be improved to take into account the limited fetch in the case of wind from the shore.

The integral (D.2) is solved numerically with the parabolic rule [Kuypers and Tinman, 1963] (based on pair-wise application of Simpson's rule), 505 intervals in first iteration, 500 increase for each subsequent iteration. The integration limits are $\omega_1 = \omega_0 + 10^{-7}$) and $\omega_2 = 1000$. Increasing the upper limit beyond $\omega_2 = 1000$ did not change the value of the integral significantly. The integral is calculated to a precision of 10^{-5}.

IMPLEMENTATION OF THE CALCULATION OF W(x,z)

The wind field W(x,z) is calculated in a rectangular, equidistantly spaced grid of Nx horizontal grid points and Nz vertical grid points. Although the actual calculation starts at the water surface, it is convenient to first look at a regular grid point well above the water surface. The grid spacings are denoted by $2\Delta x$ and $2\Delta z$ (see figure).

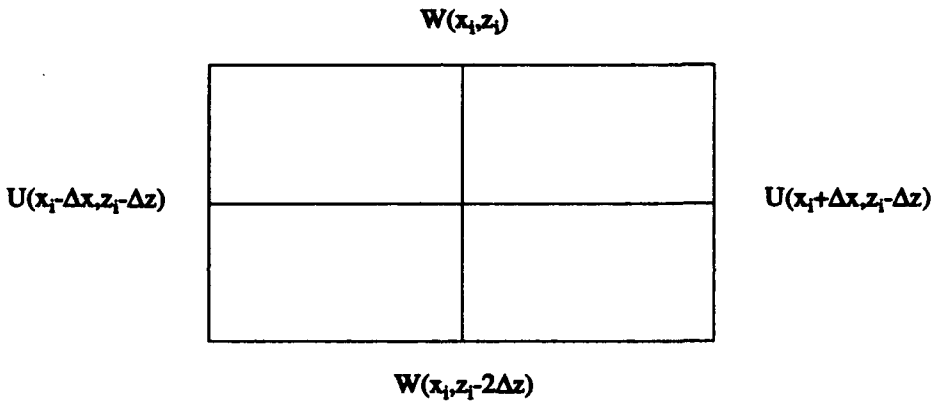

The value of W at a specific grid point (x_i,z_i) is then given by:

$$W(x_i, z_i) = W(x_i, z_i - 2\Delta z) + \Delta W \qquad \text{(E.1)}$$

where

$$\Delta W = \frac{U(x_i + \Delta x, z_i - \Delta z) - U(x_i - \Delta x, z_i - \Delta z)}{2\Delta x} \qquad \text{(E.2)}$$

Let us now turn our attention to the first grid point (x_i,z_j) that is at a height $\alpha\Delta z \leq 2\Delta z$ above the water surface $\eta(x_i)$. Close to the water surface, the gradients in U and W become large and a more dense grid is needed to correctly calculate ΔW. Therefore, $\alpha\Delta z$ is divided in 10 equidistant intervals with spacing $\Delta_1 z$. The horizontal grid is expanding with height:

$$\Delta_k x = k \Delta_1 z \qquad 1 \le k \le 10 \tag{E.3}$$

where k = 1 in the z-interval closest to the surface. For each of the 10 intervals ΔW is calculated and added to the surface value $W(x_i,\eta(x_i))$ to obtain $W(x_i,z_j)$.

A difficulty arises when one of the grid points $U(x_1 \pm \Delta x, z_1 - \Delta z)$ used to calculate ΔW is below the water surface (see figure above). In that case the grid point is neglected and ΔW is calculated from the remaining grid point:

$$\Delta W = \frac{\pm U(x_i \pm \Delta x, z_i - \Delta z) \mp U(x_i, z_i - \Delta z)}{\Delta x} \tag{E.4}$$

The large number of Nz that is needed for an accurate calculation of W(x,z) presents another numerical problem since the database of the wind field W(x,z) grows very large when both Nx and Nz are large. To keep its size within acceptable limits, W(x,z) is only calculated from the wave trough to 1 mtr above the wave crest. Even then, it is necessary to store only every n^{th} z-grid point, which results in a z-grid spacing of typically 1-5 cm in the database (depending on the wave height).[1]

The database may be used to infer W(x,z) at any location (x,z). To this end, the database is searched for the 4 entries near (x,z), see figure:

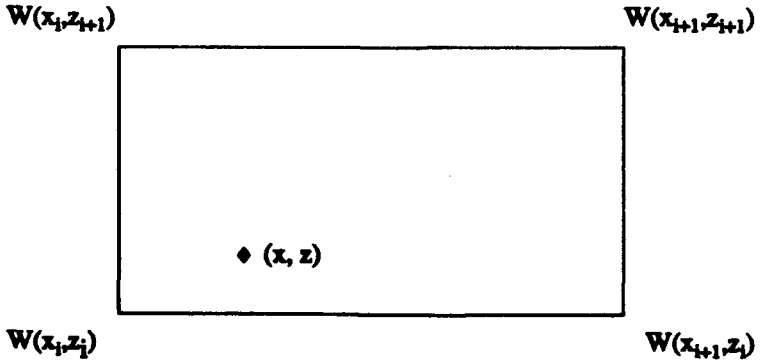

1 Note that W(x,z) depends on U_{10}, the key input variable. Therefore, databases of W(x,z) are only valid for one specific value of U_{10}.

When one of the grid points (x_i,z_j) or (x_{i+1},z_j) is in the water, W(x,z) is calculated from the water surface $(x,\eta(x))$ in the manner described above. In the other case, first $W(x,z_j)$ is calculated by 2-point interpolation in the x-direction. Subsequently, W(x,z) is calculated from $W(x,z_j)$ by the continuity equation. This method yields accurate values for W(x,z) when the x-grid is densely spaced.

Alternatively, but less accurately, a 4-point interpolation may be used to determine $W(x,z_j)$, $W(x,z_{j+1})$ and W(x,z), neglecting any missing grid points. Thus, $W(x,z_j) = W(x_i,z_j)$ when (x_{i+1},z_j) is in the water. However, in the model code this method is preferred, because it saves computation time and yields nearly identical droplet trajectories (see §4.2).

ONGERUBRICEERD

REPORT DOCUMENTATION PAGE (MOD-NL)

1. DEFENSE REPORT NUMBER (MOD-NL)	2. RECIPIENT'S ACCESSION NUMBER	3. PERFORMING ORGANIZATION REPORT NUMBER
TD93-0758		FEL-93-A035
4. PROJECT/TASK/WORK UNIT NO.	**5. CONTRACT NUMBER**	**6. REPORT DATE**
22176.1	A90KM638	AUGUST 1993
7. NUMBER OF PAGES	**8. NUMBER OF REFERENCES**	**9. TYPE OF REPORT AND DATES COVERED**
79 (INCL. 5 APPENDICES, EXCL. RDP & DISTRIBUTION LIST)	73	FINAL, JUN '91 - DEC '92

10. TITLE AND SUBTITLE
CONVERSION OF THE CLUSE MODEL FOR APPLICATIONS OVER OPEN OCEAN; PROGRESS REPORT

11. AUTHOR(S)
DR. A.M.J. VAN EIJK, DR. P.G. MESTAYER, DR. G. DE LEEUW

12. PERFORMING ORGANIZATION NAME(S) AND ADDRESS(ES)
TNO PHYSICS AND ELECTRONICS LABORATORY, P.O. BOX 96864, 2509 JG THE HAGUE
OUDE WAALSDORPERWEG 63, THE HAGUE, THE NETHERLANDS

13. SPONSORING/MONITORING AGENCY NAME(S)
ROYAL NETHERLANDS NAVY (MAIN SPONSOR TNO-FEL)

14. SUPPLEMENTARY NOTES
THE CLASSIFICATION DESIGNATION ONGERUBRICEERD IS EQUIVALENT TO UNCLASSIFIED

15. ABSTRACT (MAXIMUM 200 WORDS, 1044 POSITIONS)
THE CLUSE MODEL HAS BEEN DEVELOPED TO DESCRIBE THE DYNAMICS OF (FRESH WATER) SPRAY DROPLETS IN THE HOMOGENEOUS BOUNDARY LAYER OF AN AIR-SEA INTERACTION SIMULATION TUNNEL, AND THEIR INFLUENCE ON HUMIDITY AND TEMPERATURE PROFILES (ROUAULT ET AL., 1991). EXTENSION TO OPEN OCEAN CONDITIONS REQUIRES THAT THE FRESH WATER DROPLETS ARE REPLACED BY SEA-SALT AEROSOL, AND THAT THE INFLUENCE OF WAVES IS TAKEN INTO ACCOUNT. IN THIS REPORT WE DESCRIBE THE PROGRESS ON THE DEVELOPMENT OF THE SEACLUSE MODEL THAT APPLIES TO OPEN OCEAN CONDITIONS. THE CALCULATION OF THE PROFILES OF THE MEAN WIND VELOCITY AND TURBULENT DIFFUSIVITY HAS BEEN CHANGED TO TAKE INTO ACCOUNT THE CHARACTERISTICS OF THE MARINE ATMOSPHERE AND OF THE WAVE FIELD. A MODULE WAS ADDED TO THE INITIALIZATION ROUTINES THAT MODELS THE AIR FLOW OVER THE WAVES IN A NON-TURBULENT AND NON-EVAPORATIVE ATMOSPHERE. THIS MODULE YIELDS VERTICAL PROFILES OF DROPLET CONCENTRATIONS THAT ENTER IN THE RELAXATION TERM THAT MODELS THE MEAN MOVEMENT OF THE PARTICLES. THESE PROFILES ARE THEN MODIFIED IN THE ITERATIVE BUDGET CALCULATION THAT ACCOUNTS FOR DROPLET TRANSPORT BY ATMOSPHERIC TURBULENCE AND THEIR INTERACTION WITH THE HUMIDITY FIELD BY EVAPORATION. IN THIS PART OF THE CODE, THE EVAPORATION MODULE WAS CHANGED TO DESCRIBE THE EVAPORATION OF SEA SALT AEROSOLS IN THE MARINE ATMOSPHERE. THE OUTPUT OF THE NEW SEACLUSE MODEL CONSISTS OF VERTICAL PROFILES OF TEMPERATURE, HUMIDITY AND AEROSOL CONCENTRATION FROM THE SEA SURFACE UP TO THE TOP OF THE MARINE ATMOSPHERIC BOUNDARY LAYER.

16. DESCRIPTORS
ATMOSPHERIC MODEL
AEROSOL
ATMOSPHERIC DIFFUSION
WATER VAPOUR TRANSPORT BY EVAPORATION
MARINE ENVIRONMENT

IDENTIFIERS
CLUSE
MARINE ATMOSPHERIC BOUNDARY LAYERS
K-MODEL

17a. SECURITY CLASSIFICATION (OF REPORT)	17b. SECURITY CLASSIFICATION (OF PAGE)	17c. SECURITY CLASSIFICATION (OF ABSTRACT)
ONGERUBRICEERD	ONGERUBRICEERD	ONGERUBRICEERD

18. DISTRIBUTION/AVAILABILITY STATEMENT
UNLIMITED

17d. SECURITY CLASSIFICATION (OF TITLES)
ONGERUBRICEERD

ONGERUBRICEERD